BAGOT'S PARK, ABBOTS BROMLEY, STAFFORDSHIRE, III: Archaeomagnetic Dating Report 2002

Paul Linford and Chris Welch

Summary

Study of the remains of glassmaking sites at Bagot's Park near Abbots Bromley in Staffordshire, has revealed the presence of eighteen furnaces dating from the medieval and post-medieval period. As part of an ongoing project to investigate the evolution of glassmaking in the area, the *CfA* was asked to provide archaeomagnetic dates for the last use of each furnace. Twelve furnaces were excavated and dated in 2000 and 2001 and this work is the subject of two earlier reports (Linford 2001, Linford and Welch 2001). Two new furnace sites were investigated in 2002 and two of the previously sampled furnaces were re-excavated so that more samples could be extracted to improve their dating. The two new furnaces, 17 and 18, proved to have been disturbed by modern agricultural practice and the archaeomagnetic dates are of poor precision. However, it was possible to improve the dating of the two revisited furnaces, 6aBP and 15bBP, in the latter case obtaining a date for a furnace that had previously been undatable. Now that archaeomagnetic date ranges are available for fifteen furnaces, trends in the development of glassmaking at the site begin to emerge.

BAGOT'S PARK, ABBOTS BROMLEY, STAFFORDSHIRE, III:
Archaeomagnetic Dating Report 2002

Introduction

Until the mid-1960s Bagot's Park near Abbots Bromley in Staffordshire (SK 095 275, longitude 1.9°W, latitude 52.8°N) was an area of ancient oak trees and scrubby grazing. A programme of reclamation then ensued to convert the area into productive arable land, during which the remains of a number of glassmaking sites were recognised. One of these (now known as site 4) was excavated by David Crossley in 1966 (Crossley, 1967). He went on to identify a further 14 sites within the Park, although these were not excavated. Unfortunately, the upstanding remains of the furnaces were destroyed during the reclamation using explosives and bulldozers to remove obstacles to ploughing.

No further investigation was carried out until 1996 when Chris Welch, then Principle Archaeological Officer for the county of Staffordshire, revisited Bagot's Park. As a result of his investigations eighteen glassmaking sites have been identified within the Park dating from a period between about 1300 and 1615 AD. He instigated a project to investigate the evolution of glassmaking in Bagot's Park concentrating on: fieldwalking of the glass making sites (with the assistance of students from Keele University's Staffordshire Archaeology Summer School); geophysical survey (with the assistance of Dr. Ruth Murdie of Keele University); and limited excavation to obtain samples for archaeomagnetic dating (Welch 1997, 1998a, 1998b). The latter is essential to establish an absolute chronology for various sites within the Park against which developments in the technology of glassmaking that they exhibit can be measured. Hence, with the support of the English Heritage regional Inspector of Ancient Monuments, Paul Stamper, the Centre for Archaeology (EH C*f*A) was asked to provide archaeomagnetic dates for the features.

As Bagot's Park is under an arable management regime, it is only possible to excavate the glassmaking sites during a few weeks in late summer between the harvesting of one crop and the sowing of the next. Even during this time, the glassmaking sites are not all free of crops simultaneously. The largely volunteer excavation team can only spare a limited amount of time each year for the project, so it was decided to mount several campaigns to collect archaeomagnetic samples over successive years. An initial programme of fieldwork was carried out in September 2000 (Linford 2001), followed by a second programme in 2001 (Linford and Welch 2001). The present report describes the results of further excavations carried out between the 2nd and 4th September 2002.

Two new glassmaking sites were excavated in 2002, 17 and 18. In addition sites 6a and 15b were re-excavated as the samples previously taken from these furnaces had proven to be unsatisfactory for directional archaeomagnetic dating purposes. In all four cases it was found that most of the actual furnace remains had been destroyed when the land was reclaimed in the 1960s. What survived was fired clay that had originally lain beneath the furnaces and, in some cases, a few of the sandstone blocks that comprised the footings of the furnace trough. These latter were heavily decayed owing to exposure to intense heat during the furnaces' operation. However, in all cases there was a limited resource of material that could

confidently be identified as undisturbed and well fired, reducing the opportunities for obtaining precise archaeomagnetic dates.

All the archaeomagnetic sampling was carried out by Paul Linford with the assistance of Chris Welch and members of his volunteer team. Subsequent laboratory measurement and analysis was performed by the author.

Method

Samples were collected from glassmaking sites 6a, 15b, 17 and 18 using the disc method (see appendix, section 1a). Samples from site 17 were orientated to true north using a gyro-theodolite. The samples from the other sites were orientated using a magnetic compass, the deviation between magnetic and true north in the area having been established when the gyro-theodolite was used. To identify which glassmaking site each sample came from, all the samples numbers were prefixed by the relevant site number followed by the letters "BP" (e.g.: all samples from site 15b were prefixed with "13BBP").

The natural remanent magnetisation (NRM) measured in archaeomagnetic samples is assumed to be caused by thermoremanent magnetisation (TRM) created at the time when the feature of which they were part was last fired. However, a secondary component acquired in later geomagnetic fields can also be present, caused by diagenesis or partial reheating. Additionally, the primary TRM may be overprinted by a viscous component, depending on the grain size distribution within the magnetic material. These secondary components are usually of lower stability than the primary TRM and can thus be removed by partial demagnetisation of the samples.

A typical strategy for analysing a set archaeomagnetic samples from a fired archaeological feature is to first measure their NRM magnetisation. These NRM measurements are then inspected and one or more samples are selected for pilot partial demagnetisation. Pilot demagnetisation of a sample involves exposing it to an alternating magnetic field of fixed peak strength and measuring the resulting changes in its magnetisation. The procedure is repeated with increasing peak field strengths to build up a complete picture of the coercivity spectrum of the pilot sample. From these pilot partial demagnetisation results an optimum peak field strength is selected to be applied to the remaining samples. This optimum field strength is chosen to remove as much of the secondary magnetisation as possible whilst leaving the primary magnetisation intact. The equipment used for these measurements is described in section 2 of the appendix.

A mean TRM direction is then calculated from the partially demagnetised sample measurements. Some samples may be excluded from this calculation if their TRM directions are so anomalous as to make them statistical outliers from the overall TRM distribution. A "magnetic refraction" correction is often applied to the sample mean TRM direction to compensate for distortion of the earth's magnetic field due to the geometry of the magnetic fabric of the feature itself. Then the mean is adjusted according to the location of the feature relative to a notional central point in the UK (Meriden), so that it can be compared with UK archaeomagnetic calibration data to produce a date of last firing for the feature. Notes concerning the mean calculation and subsequent calibration can be found in sections 3 and 4 of the appendix.

This measurement and calibration strategy was applied to the analysis of the samples from Bagot's Park. As all the samples were taken from the floors of features, a magnetic refraction correction (note 3b) of 2.4° was added to the inclination of each mean TRM direction before calibration.

Results

Feature	N	Dec°	Inc°	α_{95}	k		Date Range	Comment*
6a	12	2.1 (2.1)	59.2 (58.8)	2.6	288.5	63%:	1395 – 1430 AD	Surface finds not diagnostic. Date expected to be similar to 6b (C15th AD).
						95%:	1410 – 1520 AD	
6a using both new samples and those from 2000	19	1.4 (1.5)	58.6 (58.2)	2.3	218.9	63%:	1395 – 1430 AD	
						95%:	1275 – 1320 AD	
							or 1390 – 1445 AD	
15b	16	-0.4 (-0.3)	56.8 (56.5)	4.0	85.5	63%:	1375 – 1415 AD	C16th AD date expected owing to proximity to dwelling dating from around 1520 AD.
						95%:	1290 – 1450 AD	
17	6	7.2 (7.2)	59.9 (59.6)	3.5	359.6	63%:	1250 – 1295 AD	Rough estimate based on fewer than 8 samples. Presence of brick suggests C15th or later date.
							or 1430 – 1490 AD	
						95%:	1200 – 1310 AD	
							or 1405 – 1505 AD	
18	8	13.3 (13.3)	62.2 (62.0)	4.4	159.3	63%:	1150 – 1215 AD	A similar date to 17 expected although less brick evident.
							or 1455 – 1525 AD	
						95%:	1100 – 1290 AD	
							or 1435 – 1545 AD	

Table 1; Archaeomagnetic dates inferred for features excavated at Bagot's Park in 2002. N = number of samples used to calculate mean TRM. Dec = mean declination (bracketed value is Meriden corrected). Inc = mean inclination (bracketed value is Meriden corrected). α_{95} = internal angle of cone of confidence. k = Fisher precision statistic. *Comment on expected date based upon archaeological considerations.

Table 1 summarises the mean TRM directions and the deduced date ranges for all the features sampled at Bagot's Park in September 2002. The following section provides descriptions of the features sampled and notes any important points about their archaeomagnetic analysis. TRM measurements for all samples may be found grouped by feature in the tables at the end of the report. These tables also record each sample's composition, the demagnetisation level applied to it and whether it was rejected from the feature's mean TRM calculation.

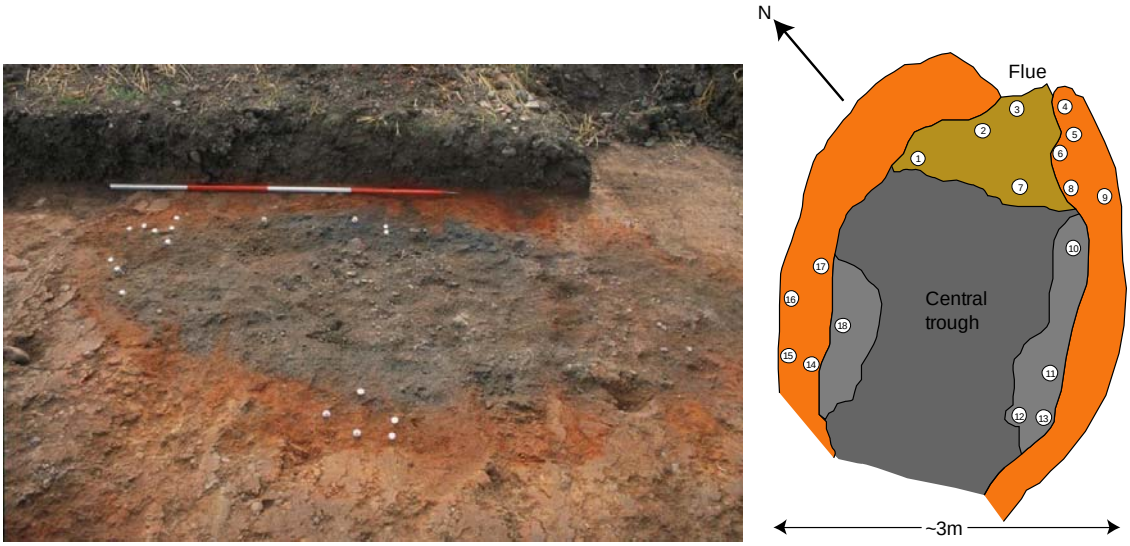

Figure 1: Photograph (left) and sketch plan (right) showing distribution of samples on fired clay areas at site 6a (sketch not to scale). The photograph is viewed from the north.

Site 6a

When originally excavated in 2000 only a small area at the western end of this furnace was exposed. This resulted in many of the samples extracted on that visit being taken from discrete areas of fired clay, near the western flue of the furnace, but not directly connected with it. These discrete areas of heating are thought to be the result of ancillary features, such as annealing furnaces, necessary to work the glass after it has been produced. However, as a result of the earlier sampling exercises, it has been found that the fired clay in these areas has invariably been disturbed, perhaps at the time the furnace was decommissioned, and thus cannot be used for directional archaeomagnetism. Hence, in 2002, the entire remains of the furnace were exposed to maximise the area available for sampling.

The approximate sample locations are depicted in Figure 1, where it can be seen that sampling was concentrated on areas at the centre and eastern end of the furnace, as the western end had been sampled in 2000. Sample measurements are recorded in Tables 2 and 3 and Figure 6 depicts the distribution of sample TRM directions before and after partial demagnetisation. Figures 7 to 9 illustrate the results of pilot demagnetisation on samples 6ABP03, 6ABP12 and 6ABP14 respectively.

Table 4 shows stability estimates for the magnetisation in these samples based upon the method of Tarling and Symons (1967). In this method, any sample with a maximum stability parameter greater than 2 is judged to record a stable TRM direction and a parameter value over 5 suggests extreme stability. The figures in Table 4 indicate that the magnetisations of all three pilot demagnetisation samples are extremely stable, with maximum stability occurring between 5 and 15mT. Based upon these statistics and Figures 7 to 9, which indicate a viscous remanent component present in domains with coercivities up to 5mT, it was decided to partially demagnetise the remaining samples in a 15mT AF field.

The distribution of TRM directions after this treatment is depicted in Figure 6b. It can be seen that 6 samples (02, 07, 10, 12, 16 and 17) have TRM directions that fall outside the main cluster even after this treatment. In the case of sample 6ABP16, the large change between its NRM

direction and TRM direction after 15mT partial demagnetisation suggests that it was not stably magnetised. However, the other 5 samples appear stable and it is likely that disturbance due to ploughing in the recent past is to blame. Certainly, grooves thought to have been caused by ploughing were observed in areas of the fired clay. Thus, all 6 samples were excluded from the mean calculated in the first row of Table 1. This mean is depicted in black in Figure 10 superimposed on the UK archaeomagnetic calibration curve.

To improve the precision of this mean, the same sample set that was used in its calculation was combined with the sample set used to produce the original date for furnace 6a in 2000 (see Linford 2001 for details). The improved mean, based upon a total of 19 samples, was used to deduce the final date range for 6a; it is listed in the second row of Table 1 and depicted in grey in Figure 10.

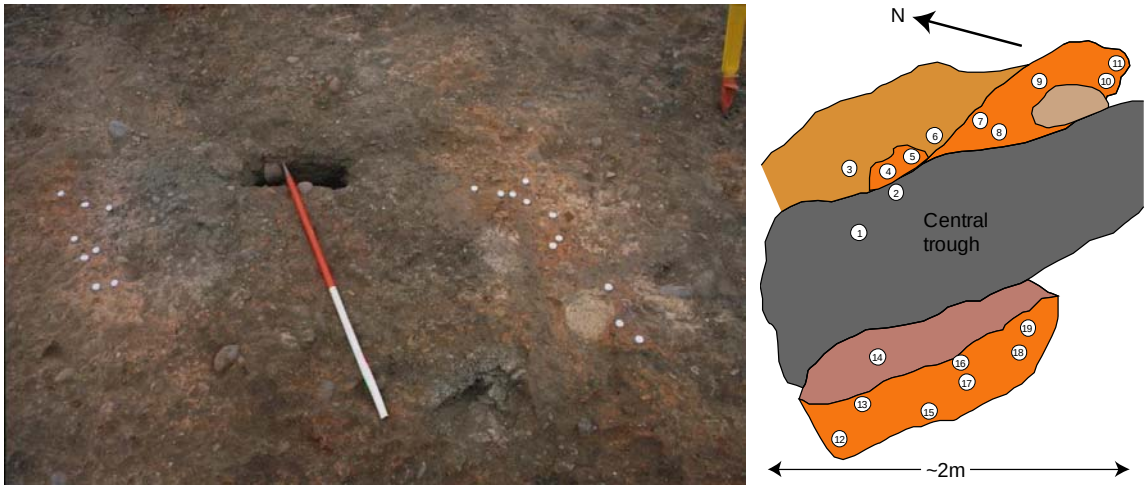

Figure 2: Photograph (left) and sketch plan (right) showing distribution of samples on fired clay areas at site 15b (sketch not to scale). The photograph is viewed from the south.

Site 15b

As with site 6a, this site had previously been sampled, this time in 2001. However, at that time, the excavation clipped only the very southern end of the feature. As a result, it was not possible to clearly identify the furnace outline and only fired clay associated with ancillary features was sampled. It was not possible to obtain an archaeomagnetic date from this material, for the reasons discussed under Site 6a above. Hence, the 2002 excavation trench was positioned to the north of the 2001 trench to uncover more of the furnace remains.

Approximate sample locations are depicted in Figure 2 and sample measurements are recorded in Tables 5 and 6. Figure 11 depicts the distribution of sample TRM directions before and after partial demagnetisation. Figures 12 to 14 illustrate the results of pilot demagnetisation on samples 15ABP01, 15BBP09 and 15BBP16 respectively. Table 7 lists the stability estimates for the magnetisation in these samples. All three appear very stable although the median destructive field values for samples 09 and 16 are low, around 10-15mT, suggesting that they had not been exposed to particularly high temperatures during the firing of the furnace. Some viscous remanence is apparent in the low coercivity domains of all three samples, so it was decided to partially demagnetise the remaining samples in a 5mT AF field. The results after this treatment are depicted in Figure 11b, where it can be seen that most of the samples form a cluster, albeit a fairly dispersed one. Samples 15BBP04, 15BBP05 and

15BBP11 appear to be outliers. This is likely to be due to disturbance by modern agriculture or whist exposing the feature for sampling as all three came from upstanding areas of the remains more likely to be caught by the plough or excavator bucket.

Hence, these three samples were excluded from the mean TRM calculation which is listed in the third row of Table 1. Figure 15 shows the comparison of this calculated mean TRM vector with the UK archaeomagnetic calibration curve.

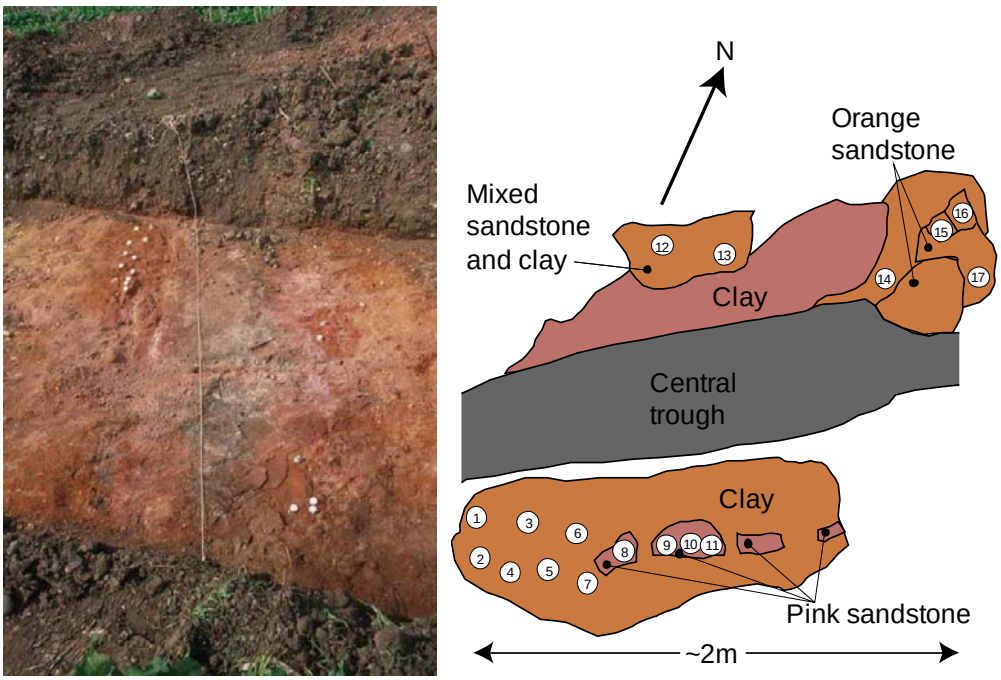

Figure 3: Photograph (left) and sketch plan (right) showing distribution of samples on fired clay areas at site 17 (sketch not to scale). The photograph is viewed from the east.

Site 17

This furnace was aligned approximately east-west and the excavation trench exposed a 2m wide section across its centre. Inspection revealed several pieces of sandstone that were the remains of the structure of the furnace itself, all much decayed owing to the heat generated during its operation.

Approximate sample locations are depicted in Figure 3 but it should be noted that samples 17BP08 and 17BP10 disintegrated during extraction. Measurements for the remaining samples are recorded in Tables 8 and 9. Figure 16 depicts the distribution of sample TRM directions before and after partial demagnetisation. Figures 17 to 19 illustrate the results of pilot demagnetisation on samples 17BP06, 17BP11 and 17BP14 respectively. Table 10 lists the stability estimates for the magnetisation in these samples. All three appear stable although 17BP14 is the least so, with a strong secondary (possibly viscous) component at coercivities up to 10mT. Hence, it was decided to demagnetise the remaining samples in a 15mT AF field to ensure removal of any such secondary components.

The results after this treatment are depicted in Figure 16b and it is clear that the TRM directions are widely scattered. This is almost certainly due to disturbance of the feature by agriculture (or possibly during excavation). The sampled pieces of sandstone certainly stood

proud of the surrounding fired clay and were thus more likely to be caught by the plough or excavator bucket. As a result it is not possible to determine a satisfactory archaeomagnetic date for the last firing of the furnace. However, an approximate date can be estimated from the 6 samples that do form a loose cluster in the centre of the distribution in Figure 16b (04, 05, 07, 09, 11 and 14). A mean TRM was calculated using just these six samples and this is listed in the fourth row of Table 1. It is depicted graphically, superimposed on the UK archaeomagnetic calibration curve in Figure 20. The poor precision of this mean is due to the small number of samples used to calculate the mean direction.

Unfortunately, the mean TRM also happens to fall close to a position occupied by the geomagnetic pole twice during the medieval period. As a result, the mean's circles of confidence intersect with two separate segments of the calibration curve and two date ranges are thus possible (see Table 1). Furthermore, it should be borne in mind that, as fewer than 8 samples have been used, the α_{95} and precision statistics are likely to be inaccurate and the deduced date ranges should not be treated with the same degree of confidence as the other Bagot's Park archaeomagnetic dates.

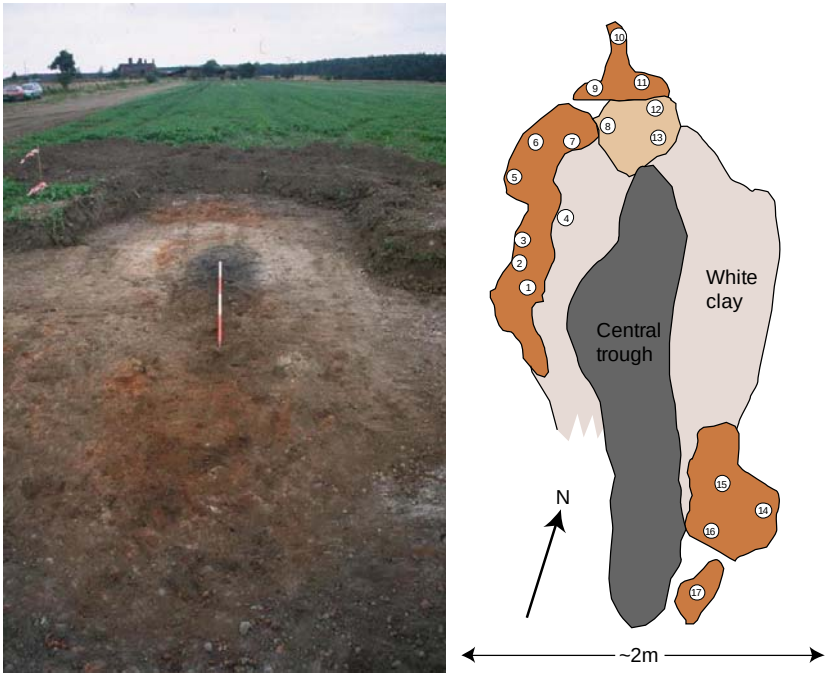

Figure 4: Photograph prior to sampling (left) and sketch plan showing distribution of samples on fired clay areas at site 18 (right, not to scale). The photograph is viewed from the south.

Site 18

A white friable sandy clay was present surrounding the remains of the central trough of this furnace. This clay type had not been observed in the remains of any of the other Bagot's Park furnaces and spot magnetic susceptibility readings suggested that it did not contain an appreciable magnetic mineral component. Thus no archaeomagnetic samples were taken from it. Figure 4 depicts the approximate locations of the samples that were taken and sample measurements are recorded in Tables 11, 12 and 13. Figure 21 depicts the distribution of sample TRM directions before and after partial demagnetisation. Figures 22 to 26 illustrate the results of pilot demagnetisation on samples 18BP03, 18BP06, 18BP08, 18BP13 and 18BP14 respectively. Table 14 lists the stability estimates for the magnetisation in these

samples. Samples 18BP03, 18BP06 and 18BP08 appear stable but samples 18BP13 and 18BP14 are not. It was concluded that these latter two samples had not been exposed to sufficient heat during the operation of the furnace to attain a stable magnetisation.

As samples 18BP03, 18BP06 and 18BP08 all exhibited a viscous component in domains with coercivities less than 10mT, the remaining samples were demagnetised in a 10mT AF field. The resulting partially demagnetised TRM vectors are depicted in Figure 21b. In this figure it can be seen that samples 18BP11 and18BP13-16 all exhibit considerable changes between their partially demagnetised TRM directions and their respective NRM values. It was concluded that these samples had not been heated sufficiently to acquire a stable magnetisation and they were excluded from the mean TRM calculation. Samples 18BP01, 18BP09, 18BP12 and 18BP17 also appear to be outliers although possessing more stable magnetisations. It is likely that these samples come from areas of the remains that have been disturbed by modern agriculture (or during excavation of the feature) and these were also excluded from the mean calculation.

A mean TRM direction was calculated from the remaining 8 samples and this is listed in the fifth row of Table 1 and depicted graphically, superimposed on the UK archaeomagnetic calibration curve in Figure 27. The poor precision of this mean is due to the small number of samples used to calculate the mean direction and the high degree of scattering in TRM directions exhibited by them. As a result, the mean's circle of confidence intersects with two separate segments of the calibration curve and two date ranges are thus possible (see Table 1).

Conclusions

The programme of excavation at Bagot's Park during 2002 has examined two previously uninvestigated glassmaking furnaces, at sites 17 and 18. Archaeomagnetic analysis has obtained dates for them but the date ranges are of poor precision. Both sites were in the same field towards the eastern end of the Park and the archaeomagnetic results suggest that the agricultural practice here has caused more disturbance to the glassmaking remains than in other areas. In addition, sites 6a and 15b, excavated in 2000 and 2001 respectively, were re-excavated to allow more archaeomagnetic samples to be taken. In the case of 6a, this has allowed an archaeomagnetic date range of improved precision to be deduced. Whilst for 15b, an archaeomagnetic date has been obtained for the first time, the samples extracted in 2001 all proving unsuitable owing to disturbance.

The date ranges derived for the last firings of the four furnaces examined during 2002 are summarised below and compared with the preliminary archaeological assessments of the sites.

Site 6a

1395 to 1430 AD at the 63% confidence level.
1275 to 1320 AD or 1390 to 1445 AD at the 95% confidence level.

This date was based upon combining samples taken in 2001 with the further samples taken this year. The earlier alternative date range at 95% confidence is due to the looping movement of the geomagnetic pole in the C14th AD (see Figure 10). Because of this, the 95% circle of confidence around the mean TRM direction intersects two segments of the calibration curve, one around the early C14th AD, the other at the end of the C14th /early

C15th AD. The archaeological evidence from surface finds is not diagnostic and the earlier date cannot be discounted on these grounds. However, the closer proximity of the mean TRM direction to the later segment of the calibration curve suggests that the later date range is more probable.

Site 15b

1375 to 1415 AD at the 63% confidence level.
1290 to 1450 AD at the 95% confidence level.

The very early start to the 95% confidence range is due to the looping movement of the geomagnetic pole in the C14th AD (see Figure 15). Thus the 95% circle of confidence around the mean TRM direction encompasses the entirety of this loop. This furnace was located in close proximity to 15a, which dates from the late C13th AD, and the remains of a dwelling which pottery suggests dates from around 1520 AD. 15b might thus be expected to be broadly contemporary with one of these two features and a late C14th/early C15th AD date is a surprise. Detailed analysis of the pottery from these features will be required to further elucidate the chronology of this area of the Park.

Site 17

1250 to 1295 AD or 1430 to 1490 AD at the 63% confidence level.
1200 to 1310 AD or 1405 to 1505 AD at the 95% confidence level.

The two possible date ranges for this feature result from the fact that the mean TRM direction falls near a crossover on the calibration curve where the geomagnetic pole occupied the same position at two different times during the medieval period (see Figure 20). Hence the circles of confidence around the mean intersect two segments of the calibration curve, one corresponding to the C13th AD, the other to the C15th AD. Finds evidence is not conclusive but tends to suggest the later date range. Quantities of brick were found in close proximity to the site and, if these relate to the furnace, dates earlier than the C15th AD can be ruled out. Furthermore, sites 17 and 18 lie in a part of the Park known as Whitemoor. This may have originated as a separate entity and was probably the *Witemore* granted by Emme Bagot to Richard Bagot in the thirteenth century, when it was described as an assart (Wrottesley 1908, p167). It was subsequently incorporated into the Park and glassmaking was unlikely to have been carried out in the area prior to this, so a date range beginning earlier than the end of the C13th AD seems improbable. Hence, for the foregoing reasons the later date range seems most likely for site 17.

Site 18

1150 to 1215 AD or 1455 to 1525 AD at the 63% confidence level.
1100 to 1290 AD or 1435 to 1545 AD at the 95% confidence level.

The two possible date ranges for this feature result from the fact that two segments of the calibration curve, one for the C12th AD the other for the early C16th AD, pass close to one another (see Figure 27). Owing to the poor precision of this archaeomagnetic date, the circles of confidence around the mean TRM direction intersect both segments. The finds tend to suggest a later date (although there was not much brick). The earliest reference to glassmakers in the area is at *Glaslone* (Glass Lane) in 1289 (Crossley 1967, p45). A furnace dating more than a century earlier than this reference would thus be surprising and so, as with site 17, the later date range seems the most likely.

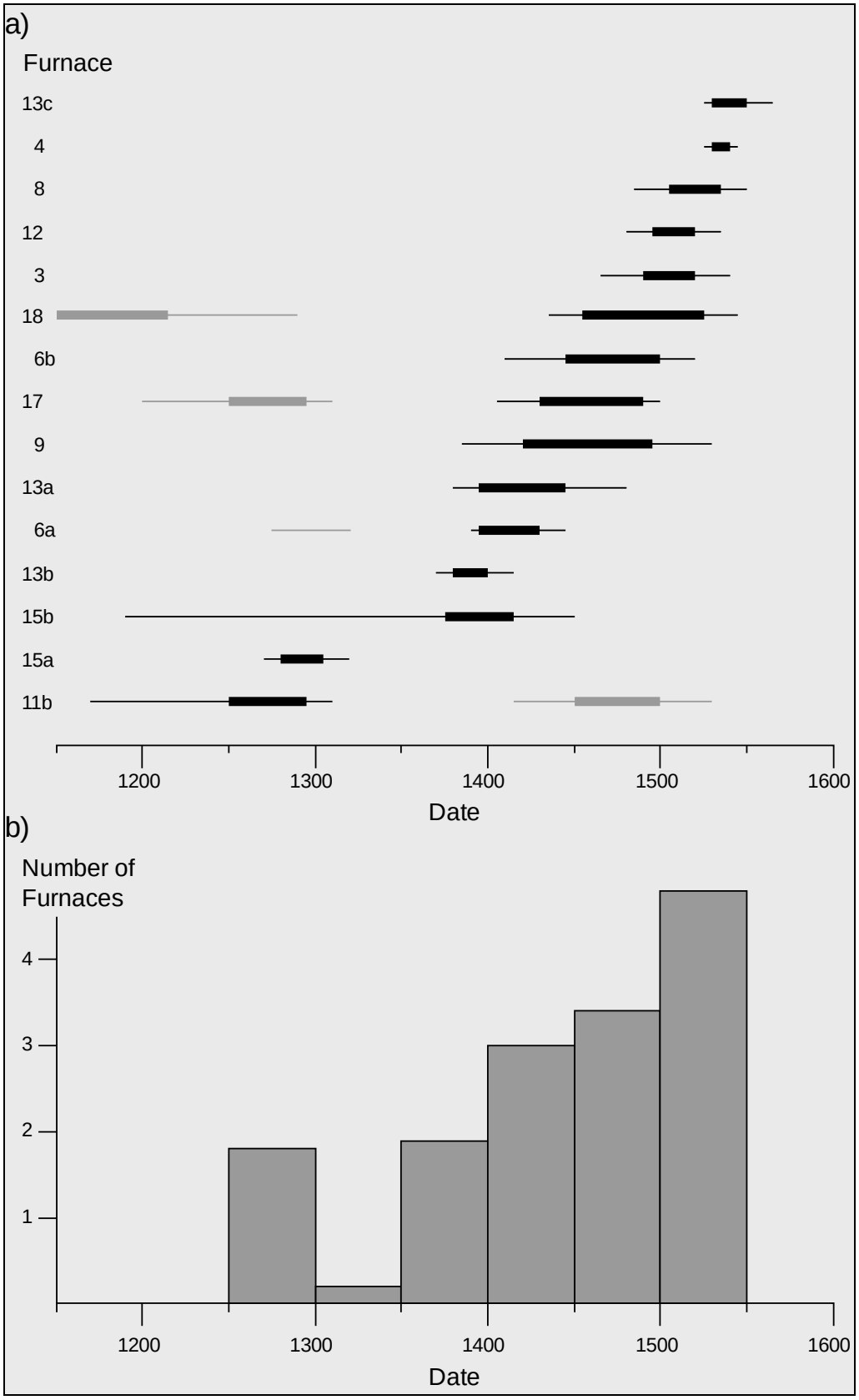

Figure 5: a) Archaeomagnetic date ranges of features from Bagot's Park. Thin lines represent 95% confidence intervals; thick lines represent 63% confidence intervals. Note the second possible date ranges for 6a, 11b, 17 and 18 shown in grey. b) Number of furnaces last fired in each 50-year period between 1250 and 1600 AD.

General discussion

In combination with the work done in previous years, a total of 15 archaeomagnetic dates have now been established for glassmaking furnaces at Bagot's Park. In the report on the 2001 sampling campaign, the relationships between all the archaeomagnetic date ranges then available was graphically illustrated (Linford and Welch 2001, Figure 7). This graph has been updated to incorporate the 2002 dates in Figure 5a. Figure 5b illustrates the distribution of the dates in a quantitative way. It shows a histogram of the number of furnaces that were last used in each 50-year period between 1250 and 1600, based on the archaeomagnetic evidence. These sums were calculated by considering each 50 year time span in turn and adding the fraction of each furnace's 63% date range that overlapped the span to its total. It should be borne in mind that the archaeomagnetic dates estimate the last firing of each furnace, hence there will be some time lag inherent in the trends indicated in the histogram.

Three other furnaces sites are known at Bagot's Park that have not been archaeomagnetically dated owing to a lack of suitable material, sites 11a, 16 and 17b. Site 11a is known from associated finds to date from the period 1583-1615 and finds at site 16 also point towards a later date. The second furnace recently noted near site 17 (provisionally labelled 17b) is thought to be contemporary with it. Hence, these dates would not greatly alter the picture of glassmaking activity indicated in Figure 5b, although site 11a does indicate that it persisted after 1550, which is the end of the latest archaeomagnetic date range.

The histogram suggests that glassmaking furnaces first appear on the site in the latter half of the 13th century AD with 2 furnaces in operation. There is then a hiatus between about 1300 and the later part of the 14th century when two more furnaces are last used. Glassmaking activity then seems to steadily increase until the turn of the 16th century AD when it peaks, with 4.8 furnaces being last used between 1500 and 1550. Further research will be required to ascertain whether this trough and peak in production can be correlated with variability in demand for glass. As yet no furnaces have been dated later than 1550 AD, although documentary evidence attests to the continuation of glassmaking at Bagot's Park until the early 17th century.

One further factor that emerges from the archaeomagnetic analysis is that furnaces in close proximity to one another do not necessarily date from the same period. This is most clearly demonstrated with the results from furnaces 13a and b, which predate 13c by a century. Furthermore, furnace 11b appears to be early in date whilst artefactual evidence suggests that 11a dates from the 1580-1615 period. Conversely, the improved date for furnace 6a suggests that it was almost contemporary with its neighbour with only 15 years between the end of its 63% date range and the start of that for 6b.

However, the most interesting archaeomagnetic dates concern site 15. Here, two furnaces have been found in close proximity to one another (15a and 15b). 15a sits within a ditched enclosure associated with a dwelling that has been dated from pottery finds to around 1520 AD. It was assumed that it would be contemporary with this cottage but the archaeomagnetic date determined in 2001 shows that it was last used in the late C13th AD. 15b was also expected to give a C16th AD Tudor date but the archaeomagnetic date described above shows that it was last used in the very early C15th AD. The separation in date of almost a century between the two furnaces is also interesting as this period brackets the apparent C14th hiatus in glassmaking activity. The results suggest that after abandoning 15a, perhaps because of the changing interests of the owners of the Park, the glassmakers reoccupied the same site on their return some 70-100 years later. Further, more detailed, analysis of the archaeological

finds from this site will be required to establish the relationships, if any, between the glassmaking furnaces and the Tudor dwelling.

P. Linford
Archaeometry Branch,
Centre for Archaeology, English Heritage.

C. Welch
Inspector of Ancient Monuments
English Heritage, South Eastern Region

Date of report: 03/12/2002

Archaeomagnetic Date Summary

Archaeomagnetic ID:	**6ABP**
Feature:	**Bagot's Park, site 6a**
Location:	**Longitude 1.9°W, Latitude 52.8°N**
Number of Samples (taken/used in mean):	**31/19**
AF Demagnetisation Applied:	**15mT**
Distortion Correction Applied:	**+2.4 °**
Declination (at Meriden):	**2.1° (2.1°)**
Inclination (at Meriden):	**59.2° (58.8 °)**
Alpha-95:	**2.6°**
k:	**288.5**
Date range (63% confidence):	**1395 AD to 1430 AD**
Date range (95% confidence):	**1275 AD to 1320 AD or 1390 AD to 1445 AD**

Archaeomagnetic ID:	**15BBP**
Feature:	**Bagot's Park, site 15b**
Location:	**Longitude 1.9°W, Latitude 52.8°N**
Number of Samples (taken/used in mean):	**19/16**
AF Demagnetisation Applied:	**5mT**
Distortion Correction Applied:	**+2.4 °**
Declination (at Meriden):	**-0.4° (-0.3°)**
Inclination (at Meriden):	**56.8° (56.5 °)**
Alpha-95:	**4.0°**
k:	**85.5**
Date range (63% confidence):	**1375 AD to 1415 AD**
Date range (95% confidence):	**1290 AD to 1450 AD**

Archaeomagnetic ID:	**17BP**
Feature:	**Bagot's Park, site 17**
Location:	**Longitude 1.9°W, Latitude 52.8°N**
Number of Samples (taken/used in mean):	**15/6**
AF Demagnetisation Applied:	**15mT**
Distortion Correction Applied:	**+2.4 °**
Declination (at Meriden):	**7.2° (7.2°)**
Inclination (at Meriden):	**59.9° (59.6 °)**
Alpha-95:	**3.5°**
k:	**359.6**
Date range (63% confidence):	**1250 AD to 1295 AD or 1430 AD to 1490 AD**
Date range (95% confidence):	**1200 AD to 1310 AD or 1405 AD to 1505 AD**

Archaeomagnetic ID:	**18BP**
Feature:	**Bagot's Park, site 18**
Location:	**Longitude 1.9^{o}W, Latitude 52.8^{o}N**
Number of Samples (taken/used in mean):	**17/8**
AF Demagnetisation Applied:	**10mT**
Distortion Correction Applied:	**+2.4 ^{o}**
Declination (at Meriden):	**13.3^{o} (13.3^{o})**
Inclination (at Meriden):	**62.2^{o} (62.0 ^{o})**
Alpha-95:	**4.4^{o}**
k:	**159.3**
Date range (63% confidence):	**1150 AD to 1215 AD or 1455 AD to 1525 AD**
Date range (95% confidence):	**1100 AD to 1290 AD or 1435 AD to 1545 AD**

	NRM Measurements				After Partial Demagnetisation			
Sample	Material	Dec°	Inc°	J(mAm^{-1})	AF(mT)	Dec°	Inc°	J(mAm^{-1})	R
6ABP01	Clay	-0.8	63.4	16039.4	15.0	-2.4	61.8	14604.8	
6ABP02	Clay	-41.8	69.3	452.1	15.0	-53.2	70.5	314.7	R
6ABP03	Clay	1.6	53.3	2074.0	15.0	4.3	54.3	1564.2	
6ABP04	Clay	-4.0	52.0	5720.9	15.0	-4.0	52.7	4147.4	
6ABP05	Clay	13.5	57.8	1154.0	15.0	14.7	57.2	823.1	
6ABP06	Clay	0.4	56.4	1193.6	15.0	-1.5	55.5	776.3	
6ABP07	Clay	-30.4	49.1	32.2	15.0	-27.4	60.0	27.0	R
6ABP08	Clay	0.7	56.1	2220.3	15.0	0.3	55.6	1411.4	
6ABP09	Clay	-6.9	56.8	303.7	15.0	-7.0	58.0	100.5	
6ABP10	Clay	-164.6	36.4	2264.7	15.0	-164.1	35.8	2176.7	R
6ABP11	Clay	-0.1	49.9	1333.2	15.0	0.3	50.1	1258.4	
6ABP12	Clay	21.6	69.4	23238.2	15.0	19.0	69.3	23364.7	R
6ABP13	Clay	6.2	53.9	5213.0	15.0	6.0	53.5	5000.8	
6ABP14	Clay	4.1	63.4	446.0	15.0	3.7	60.8	303.9	
6ABP15	Clay	7.5	60.3	1138.2	15.0	6.3	58.1	367.1	
6ABP16	Clay	-41.4	65.9	709.2	15.0	-45.8	56.7	238.1	R
6ABP17	Clay	-105.5	64.5	191.5	15.0	-126.3	60.6	67.1	R
6ABP18	Clay	4.6	61.9	634.0	15.0	4.8	62.2	605.0	

Table 2: NRM measurements of samples and measurements after partial AF demagnetisation for feature 6ABP. J = magnitude of magnetisation vector; AF = peak alternating field strength of demagnetising field; R = sample rejected from mean calculation.

	6ABP03			6ABP12			6ABP14		
AF(mT)	Dec°	Inc°	J(mAm^{-1})	Dec°	Inc°	J(mAm^{-1})	Dec°	Inc°	J(mAm^{-1})
0.0	5.2	55.7	2092.9	18.9	69.2	24459.8	5.2	63.6	480.2
1.0	4.7	55.5	2077.9	18.5	69.1	24494.8	4.8	63.0	477.0
2.5	4.5	55.3	2058.7	18.5	69.2	24481.1	4.3	62.5	469.4
5.0	4.5	55.2	2013.7	18.9	69.2	24288.4	4.1	61.9	452.5
10.0	4.0	54.8	1849.2	18.9	69.3	23971.0	3.7	61.1	385.1
15.0	4.3	54.3	1564.2	19.0	69.3	23364.7	3.7	60.8	303.9
20.0	5.0	54.6	1178.3	19.2	69.4	22539.4	4.3	60.6	226.4
30.0	5.4	54.3	618.9	18.3	68.9	19066.0	6.0	61.2	133.4
50.0	5.7	53.0	312.4	18.3	69.0	9844.6	5.4	63.4	75.8
75.0	-	-	-	15.2	69.3	3631.8	-	-	-
100.0	-	-	-	12.1	69.2	1518.6	-	-	-

Table 3: Incremental partial demagnetisation measurements for samples 6ABP03, 6ABP12 and 6ABP14.

Sample	Range min. (mT)	Range max. (mT)	Max. Stability	Dec°	Inc°
6ABP03	1.0	5.0	38.1	4.6	55.3
6ABP12	5.0	15.0	163.3	18.9	69.3
6ABP14	10.0	20.0	33.0	3.9	60.8

Table 4: Assessment of the range of demagnetisation values over which each sample attained its maximum directional stability for feature 6ABP, using the method of Tarling and Symons (1967). The declination and inclination values quoted are for the mean TRM direction for the sample calculated for all demagnetisation measurements in its range of maximum stability.

	NRM Measurements				After Partial Demagnetisation			
Sample	Material	Dec°	Inc°	J(mAm^{-1})	AF(mT)	Dec°	Inc°	J(mAm^{-1})	R
15BBP01	Clay	-6.3	53.8	21034.8	5.0	-5.9	53.5	21470.3	
15BBP02	Clay	22.1	58.9	16402.7	5.0	22.5	58.5	16036.4	
15BBP03	Clay	-4.0	42.8	27.9	5.0	-8.1	40.8	24.9	
15BBP04	Clay	-130.2	70.6	1157.4	5.0	-140.1	71.8	1068.6	R
15BBP05	Clay	29.1	53.0	257.1	5.0	40.6	45.6	190.6	R
15BBP06	Clay	-17.0	62.9	1631.2	5.0	-17.9	62.5	1546.5	
15BBP07	Clay	-20.5	56.0	2653.5	5.0	-21.1	53.5	2258.7	
15BBP08	Clay	-1.4	64.4	162.4	5.0	-0.8	64.6	135.4	
15BBP09	Clay	-12.6	61.5	1940.3	5.0	-12.7	60.3	1565.8	
15BBP10	Clay	-0.2	55.8	1907.1	5.0	0.4	53.4	1549.2	
15BBP11	Clay	-46.8	35.2	44.1	5.0	-48.9	32.1	31.8	R
15BBP12	Clay	8.7	53.8	1569.3	5.0	7.5	52.8	1258.5	
15BBP13	Clay	14.6	51.5	978.2	5.0	14.5	51.4	895.5	
15BBP14	Clay	5.5	56.9	10545.7	5.0	4.6	57.0	10007.8	
15BBP15	Clay	5.4	53.8	1132.1	5.0	1.9	53.3	885.7	
15BBP16	Clay	3.2	48.7	3677.2	5.0	1.9	47.5	3108.0	
15BBP17	Clay	6.2	55.9	1875.6	5.0	7.0	54.1	1479.1	
15BBP18	Clay	-0.6	51.4	188.7	5.0	-8.7	44.5	159.7	
15BBP19	Clay	8.4	55.6	257.1	5.0	9.0	55.5	224.0	

Table 5: NRM measurements of samples and measurements after partial AF demagnetisation for feature 15BBP. J = magnitude of magnetisation vector; AF = peak alternating field strength of demagnetising field; R = sample rejected from mean calculation.

	15BBP01			15BBP09			15BBP16		
AF(mT)	Dec°	Inc°	J(mAm^{-1})	Dec°	Inc°	J(mAm^{-1})	Dec°	Inc°	J(mAm^{-1})
0.0	-5.8	53.9	21811.1	-10.9	63.6	1911.3	3.0	49.9	3597.6
1.0	-5.8	53.7	21774.0	-11.8	62.4	1873.4	2.7	49.2	3550.7
2.5	-5.9	53.7	21674.7	-11.8	61.4	1819.5	2.5	48.4	3421.1
5.0	-5.9	53.5	21470.3	-12.7	60.3	1565.8	1.9	47.5	3108.0
7.5	-	-	-	-12.6	59.5	1153.6	1.3	47.0	2711.4
10.0	-6.0	53.4	20458.3	-13.0	58.7	718.1	0.7	46.5	2313.5
15.0	-5.8	53.1	18453.0	-9.0	62.0	279.5	0.0	45.8	1621.4
20.0	-5.6	52.8	15571.6	-18.6	66.4	116.9	-0.6	45.4	1100.9
30.0	-6.0	52.4	9979.6	4.2	57.7	66.4	0.1	46.4	490.8
50.0	-6.2	52.4	5518.3	-	-	-	-	-	-
75.0	-4.3	53.6	4707.9	-	-	-	-	-	-

Table 6: Incremental partial demagnetisation measurements for samples 15BBP01, 15BBP09 and 15BBP16.

Sample	Range min. (mT)	Range max. (mT)	Max. Stability	Dec°	Inc°
15BBP01	1.0	10.0	60.2	-5.9	53.6
15BBP09	5.0	10.0	8.8	-12.8	59.5
15BBP16	10.0	30.0	22.2	0.0	46.0

Table 7: Assessment of the range of demagnetisation values over which each sample attained its maximum directional stability for feature 15BBP, using the method of Tarling and Symons (1967). The declination and inclination values quoted are for the mean TRM direction for the sample calculated for all demagnetisation measurements in its range of maximum stability.

	NRM Measurements				After Partial Demagnetisation			
Sample	Material	Dec°	Inc°	J(mAm^{-1})	AF(mT)	Dec°	Inc°	J(mAm^{-1})	R
17BP01	Clay	-109.9	-9.4	122.4	15.0	-119.3	-5.8	38.6	R
17BP02	Clay	-9.9	-23.9	200.7	15.0	-9.3	-27.7	94.1	R
17BP03	Clay	118.9	88.3	822.2	15.0	63.1	89.5	466.3	R
17BP04	Clay	2.2	60.2	5414.0	15.0	1.7	59.9	2271.2	
17BP05	Clay	9.0	62.7	1545.7	15.0	6.2	63.1	978.5	
17BP06	Clay	11.7	37.2	1743.3	15.0	11.4	36.3	850.7	R
17BP07	Clay	9.4	56.7	1012.5	15.0	10.2	57.4	439.8	
17BP09	Sandstone	4.3	57.8	1150.9	15.0	5.2	57.5	855.8	
17BP11	Sandstone	6.9	55.1	1478.3	15.0	6.1	54.3	938.3	
17BP12	Sandstone	-53.1	68.1	41.0	15.0	-69.4	68.4	32.3	R
17BP13	Sandstone	-32.9	36.4	310.0	15.0	-32.8	33.4	271.5	R
17BP14	Sandstone	27.6	53.0	756.5	15.0	12.5	52.5	507.4	
17BP15	Sandstone	-43.3	75.8	2569.7	15.0	-44.4	75.5	1833.2	R
17BP16	Sandstone	-63.1	68.4	3182.9	15.0	-60.9	67.0	2335.7	R
17BP17	Sandstone	36.2	40.0	23127.0	15.0	36.4	38.9	12537.1	R

Table 8: NRM measurements of samples and measurements after partial AF demagnetisation for feature 17BP. J = magnitude of magnetisation vector; AF = peak alternating field strength of demagnetising field; R = sample rejected from mean calculation.

	17BP06			17BP11			17BP14		
AF(mT)	Dec°	Inc°	J(mAm^{-1})	Dec°	Inc°	J(mAm^{-1})	Dec°	Inc°	J(mAm^{-1})
0.0	11.9	38.8	1740.5	6.0	55.7	1460.2	32.1	57.0	761.1
1.0	11.8	38.2	1726.7	5.2	54.8	1455.4	31.1	56.2	753.2
2.5	11.6	37.7	1704.8	5.4	54.6	1435.8	30.2	55.9	742.4
5.0	12.2	37.4	1641.4	5.6	54.4	1388.2	28.3	55.3	714.8
10.0	12.1	36.9	1295.2	5.9	54.4	1206.0	19.0	52.9	628.0
15.0	11.4	36.3	850.7	6.1	54.3	938.3	12.5	52.5	507.4
20.0	11.9	36.6	482.6	6.2	54.2	749.1	9.5	53.1	382.3
30.0	9.3	36.5	163.0	6.3	53.9	495.6	8.3	51.8	232.3
50.0	-	-	-	5.3	54.1	330.6	1.9	50.4	115.1

Table 9: Incremental partial demagnetisation measurements for samples 17BP06, 17BP11 and 17BP14.

Sample	Range min. (mT)	Range max. (mT)	Max. Stability	Dec°	Inc°
17BP06	10.0	20.0	24.0	11.8	36.6
17BP11	10.0	20.0	74.7	6.1	54.3
17BP14	15.0	30.0	8.3	10.1	52.5

Table 10: Assessment of the range of demagnetisation values over which each sample attained its maximum directional stability for feature 17BP, using the method of Tarling and Symons (1967). The declination and inclination values quoted are for the mean TRM direction for the sample calculated for all demagnetisation measurements in its range of maximum stability.

	NRM Measurements				After Partial Demagnetisation			
Sample	Material	Dec°	Inc°	J(mAm^{-1})	AF(mT)	Dec°	Inc°	J(mAm^{-1})	R
18BP01	Clay	43.2	67.6	178.3	10.0	45.1	68.7	127.2	R
18BP02	Clay	17.3	66.1	165.2	10.0	18.9	66.2	111.0	
18BP03	Clay	16.7	60.4	1525.7	10.0	15.0	59.2	1001.8	
18BP04	Clay	5.2	62.4	96.1	10.0	1.3	61.4	84.3	
18BP05	Clay	20.8	51.3	379.9	10.0	21.0	51.5	280.0	
18BP06	Clay	12.9	53.8	774.8	10.0	15.1	53.4	669.9	
18BP07	Clay	11.8	60.6	1864.7	10.0	12.3	60.2	1680.9	
18BP08	Clay	4.0	67.1	84.5	10.0	7.2	68.2	65.1	
18BP09	Clay	28.8	42.6	90.3	10.0	33.4	38.5	51.2	R
18BP10	Clay	13.6	58.8	140.0	10.0	11.8	57.5	87.4	
18BP11	Clay	169.4	-13.3	16.4	10.0	178.5	-26.6	14.9	R
18BP12	Clay	-22.3	59.5	144.3	10.0	-25.1	59.5	114.5	R
18BP13	Clay	0.4	50.1	47.6	10.0	32.6	67.2	43.1	R
18BP14	Clay	32.7	62.8	80.1	10.0	71.1	60.7	20.3	R
18BP15	Clay	-125.0	76.2	34.7	10.0	168.6	72.3	26.5	R
18BP16	Clay	-12.4	79.6	16.4	10.0	-99.9	76.6	10.4	R
18BP17	Clay	-94.5	70.1	73.1	10.0	-95.0	69.6	70.3	R

Table 11: NRM measurements of samples and measurements after partial AF demagnetisation for feature 18BP. J = magnitude of magnetisation vector; AF = peak alternating field strength of demagnetising field; R = sample rejected from mean calculation.

	18BP03			18BP06			18BP08		
AF(mT)	Dec°	Inc°	J(mAm^{-1})	Dec°	Inc°	J(mAm^{-1})	Dec°	Inc°	J(mAm^{-1})
0.0	18.3	61.2	1527.7	13.0	53.4	775.6	5.2	68.2	88.3
1.0	17.7	61.0	1520.6	13.3	53.5	772.9	6.7	69.4	86.6
2.5	17.1	61.4	1492.0	13.4	53.5	766.7	7.0	69.0	83.9
5.0	17.3	61.0	1397.6	14.2	53.5	752.1	7.8	69.2	79.4
7.5	-	-	-	-	-	-	7.9	68.2	73.0
10.0	15.0	59.2	1001.8	15.1	53.4	669.9	7.2	68.2	65.1
15.0	15.8	59.2	571.1	13.3	53.2	542.0	7.2	68.4	43.6
20.0	15.7	59.4	330.7	13.7	53.1	411.3	1.2	67.0	27.7
30.0	16.3	60.5	154.8	14.6	53.2	198.5	-11.4	67.3	13.7
50.0	-	-	-	23.1	48.8	39.5	-	-	-

Table 12: Incremental partial demagnetisation measurements for samples 18BP03, 18BP06 and 18BP08.

	18BP13			18BP14		
AF(mT)	Dec°	Inc°	J(mAm^{-1})	Dec°	Inc°	J(mAm^{-1})
0.0	-2.6	55.5	53.4	25.5	64.6	79.0
1.0	-1.4	54.8	51.1	26.7	61.1	73.2
2.5	1.2	55.8	48.4	29.4	59.0	67.3
5.0	8.2	59.2	46.3	35.7	57.9	51.0
7.5	19.5	64.9	45.8	49.9	59.2	32.5
10.0	32.6	67.2	43.1	71.1	60.7	20.3
15.0	62.4	68.2	32.3	135.9	50.0	10.9
20.0	92.3	60.6	21.6	157.7	47.7	6.8
30.0	117.6	35.5	11.4	-	-	-
50.0	122.1	9.1	7.1	-	-	-

Table 13: Incremental partial demagnetisation measurements for samples 18BP13 and 18BP14.

Sample	Range min. (mT)	Range max. (mT)	Max. Stability	Dec°	Inc°
18BP03	10.0	20.0	39.8	15.5	59.3
18BP06	1.0	30.0	37.3	13.9	53.3
18BP08	7.5	15.0	45.8	7.4	68.3
18BP13	0.0	2.5	4.1	-0.9	55.4
18BP14	1.0	5.0	2.2	30.7	59.4

Table 14: Assessment of the range of demagnetisation values over which each sample attained its maximum directional stability for feature 18BP, using the method of Tarling and Symons (1967). The declination and inclination values quoted are for the mean TRM direction for the sample calculated for all demagnetisation measurements in its range of maximum stability.

Appendix: Standard Procedures for Sampling and Measurement

1) Sampling

One of three sampling techniques is employed depending on the consistency of the material (Clark, Tarling and Noel 1988):

a) **Consolidated materials:** Rock and fired clay samples are collected by the disc method. Several small levelled plastic discs are glued to the feature, marked with an orientation line related to True North, then removed with a small piece of the material attached.

b) **Unconsolidated materials:** Sediments are collected by the tube method. Small pillars of the material are carved out from a prepared platform, then encapsulated in levelled plastic tubes using plaster of Paris. The orientation line is then marked on top of the plaster.

c) **Plastic materials:** Waterlogged clays and muds are sampled in a similar manner to method 1b) above; however, the levelled plastic tubes are pressed directly into the material to be sampled.

2) Physical Analysis

a) Magnetic remanences are measured using a slow speed spinner fluxgate magnetometer (Molyneux et al. 1972; see also Tarling 1983, p84; Thompson and Oldfield 1986, p52).

b) Partial demagnetisation is achieved using the alternating magnetic field method (As 1967; Creer 1959; see also Tarling 1983, p91; Thompson and Oldfield 1986, p59), to remove viscous magnetic components if necessary. Demagnetising fields are measured in milli-Tesla (mT), figures quoted being for the peak value of the field.

3) Remanent Field Direction

a) The remanent field direction of a sample is expressed as two angles, declination (Dec) and inclination (Inc), both quoted in degrees. Declination represents the bearing of the field relative to true north, angles to the east being positive; inclination represents the angle of dip of this field.

b) Aitken and Hawley (1971) have shown that the angle of inclination in measured samples is likely to be distorted owing to magnetic refraction. The phenomenon is not well understood but is known to depend on the position the samples occupied within the structure. The corrections recommended by Aitken and Hawley are applied, where appropriate, to measured inclinations, in keeping with the practise of Clark, Tarling and Noel (1988).

c) Individual remanent field directions are combined to produce the mean remanent field direction using the statistical method developed by R. A. Fisher (1953). The quantity α_{95}, "alpha-95", is quoted with mean field directions and is a measure of the precision of the determination (see Aitken 1990, p247). It is analogous to the standard error statistic for scalar quantities; hence the smaller its value, the better the precision of the date.

d) For the purposes of comparison with standardised UK calibration data, remanent field directions are adjusted to the values they would have had if the feature had been located at Meriden, a standard reference point. The adjustment is done using the method suggested by Noel (Tarling 1983, p116).

4) Calibration

a) Material less than 3000 years old is dated using the archaeomagnetic calibration curve compiled by Clark, Tarling and Noel (1988).

b) Older material is dated using the lake sediment data compiled by Turner and Thompson (1982).

c) Dates are normally given at the 63% and 95% confidence levels. However, the quality of the measurement and the estimated reliability of the calibration curve for the period in question are not taken into account, so this figure is only approximate. Owing to crossovers and contiguities in the curve, alternative dates are sometimes given. It may be possible to select the correct alternative using independent dating evidence.

d) As the thermoremanent effect is reset at each heating, all dates for fired material refer to the final heating.

e) Dates are prefixed by "cal", for consistency with the new convention for calibrated radiocarbon dates (Mook 1986).

References

Aitken, M. J. 1990. *Science-based Dating in Archaeology*. London: Longman.

Aitken, M. J. and Hawley, H. N. 1971. Archaeomagnetism: evidence for magnetic refraction in kiln structures. *Archaeometry* **13**, 83-85.

As, J. A. 1967. The A.C. demagnetisation technique, in *Methods in Palaeomagnetism*, D. W. Collinson, K. M. Creer and S. K. Runcorn (eds). Amsterdam: Elsevier.

Clark, A. J., Tarling, D. H. and Noel, M. 1988. Developments in Archaeomagnetic Dating in Britain. *J. Arch. Sci.* **15**, 645-667.

Creer, K. M. 1959. A.C. demagnetisation of unstable Triassic Keuper Marls from S. W. England. *Geophys. J. R. Astr. Soc.* **2**, 261-275.

Crossley, D. W. 1967. Glassmaking in Bagot's Park Staffordshire, in the Sixteenth Century. *Post Medieval Archaeology* **1**, 44-83.

Fisher, R. A. 1953. Dispersion on a sphere. *Proc. R. Soc. London A* **217**, 295-305.

Linford, P. 2001. Bagot's Park, Abbots Bromley, Staffordshire. Archaeomagnetic Dating Report, 2001. Centre for Archaeology Report **17/2001**.

Linford, P. and Welch, C. 2001. Bagot's Park, Abbots Bromley, Staffordshire, II. Archaeomagnetic Dating Report, 2001. Centre for Archaeology Report **87/2001**.

Molyneux, L., R. Thompson, R., Oldfield, F. and McCallan, M. E. 1972. Rapid measurement of the remanent magnetisation of long cores of sediment. *Nature* **237**, 42-43.

Mook, W. G. 1986. Recommendations/Resolutions Adopted by the Twelfth International Radiocarbon Conference. *Radiocarbon* **28**, M. Stuiver and S. Kra (eds), 799.

Tarling, D. H. 1983. *Palaeomagnetism*. London: Chapman and Hall.

Tarling, D. H. and Symons, D. T. A. 1967. A stability index of remanence in palaeomagnetism. *Geophys. J. R. Astr. Soc*. **12**, 443-448.

Thompson, R. and Oldfield, F. 1986. *Environmental Magnetism*. London: Allen and Unwin.

Turner, G. M. and Thompson, R. 1982. Detransformation of the British geomagnetic secular variation record for Holocene times. *Geophys. J. R. Astr. Soc.* **70**, 789-792.

Welch, C. 1997. Glassmaking sites in Bagot's Park, Staffordshire. *West Midlands Archaeology* **40**, 8-12.

Welch, C. 1998a. Bagot's Park, Abbots Bromley, Staffordshire. Investigation of ancient glassmaking sites. Interim report on work carried out in September-October 1998. *Unpublished report*.

Welch, C. 1998b. Bagot's Park Glassmaking: fieldwork in 1998. *West Midlands Archaeology*, **41**, 70-72.

Wrottesley, G. 1908. 'History of the Bagot Family' in *Collections for a History of Staffordshire* vol. ix.

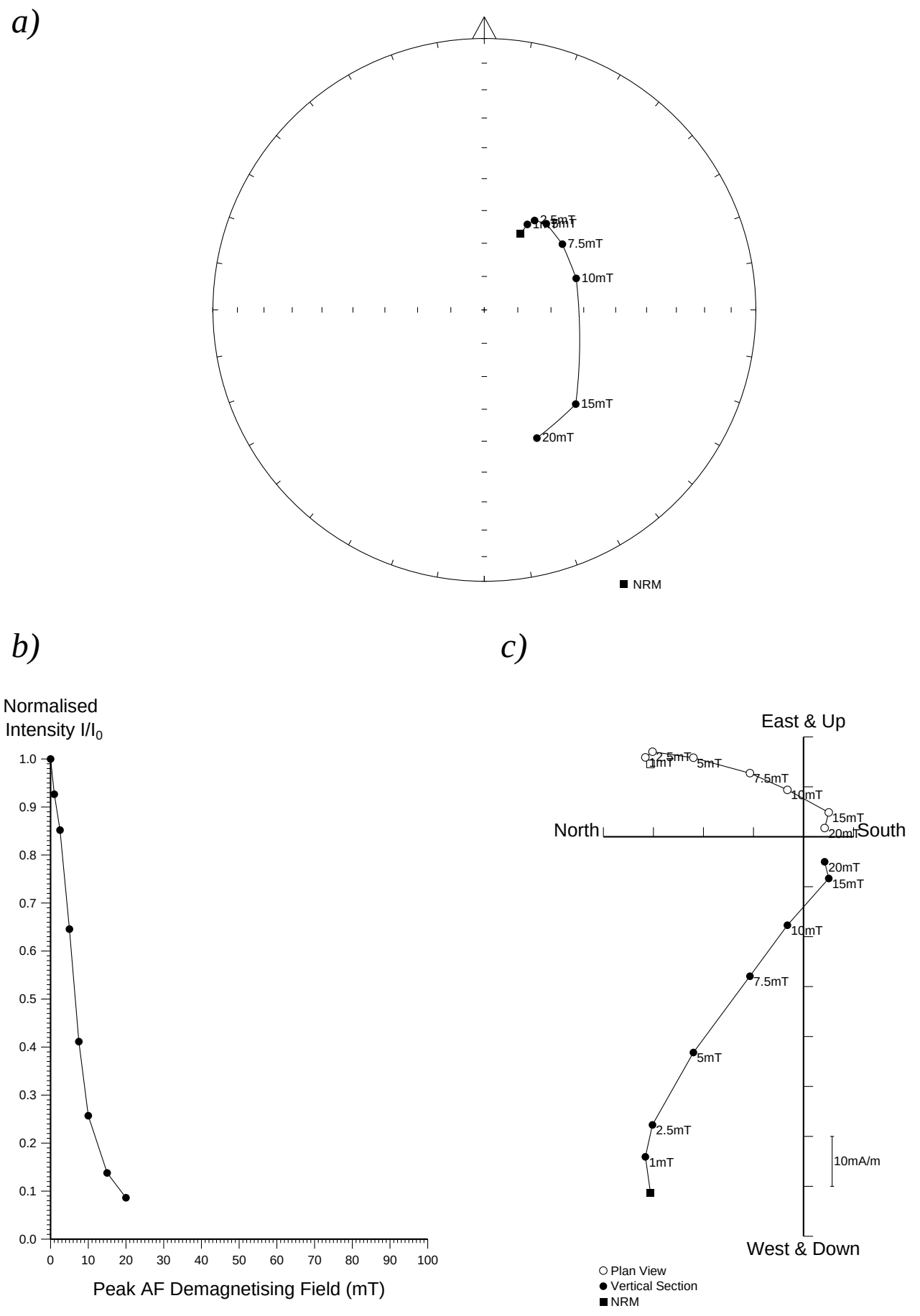

Figure 26: Stepwise AF demagnetisation of sample 18BP14. Diagram a) depicts the variation of the remanent direction as an equal area stereogram (declination increases clockwise, while inclination increases from zero at the equator to 90 degrees at the centre of the projection); b) shows the normalised change in remanence intensity as a function of the demagnetising field; c) shows the changes in both direction and intensity as a vector endpoint projection.

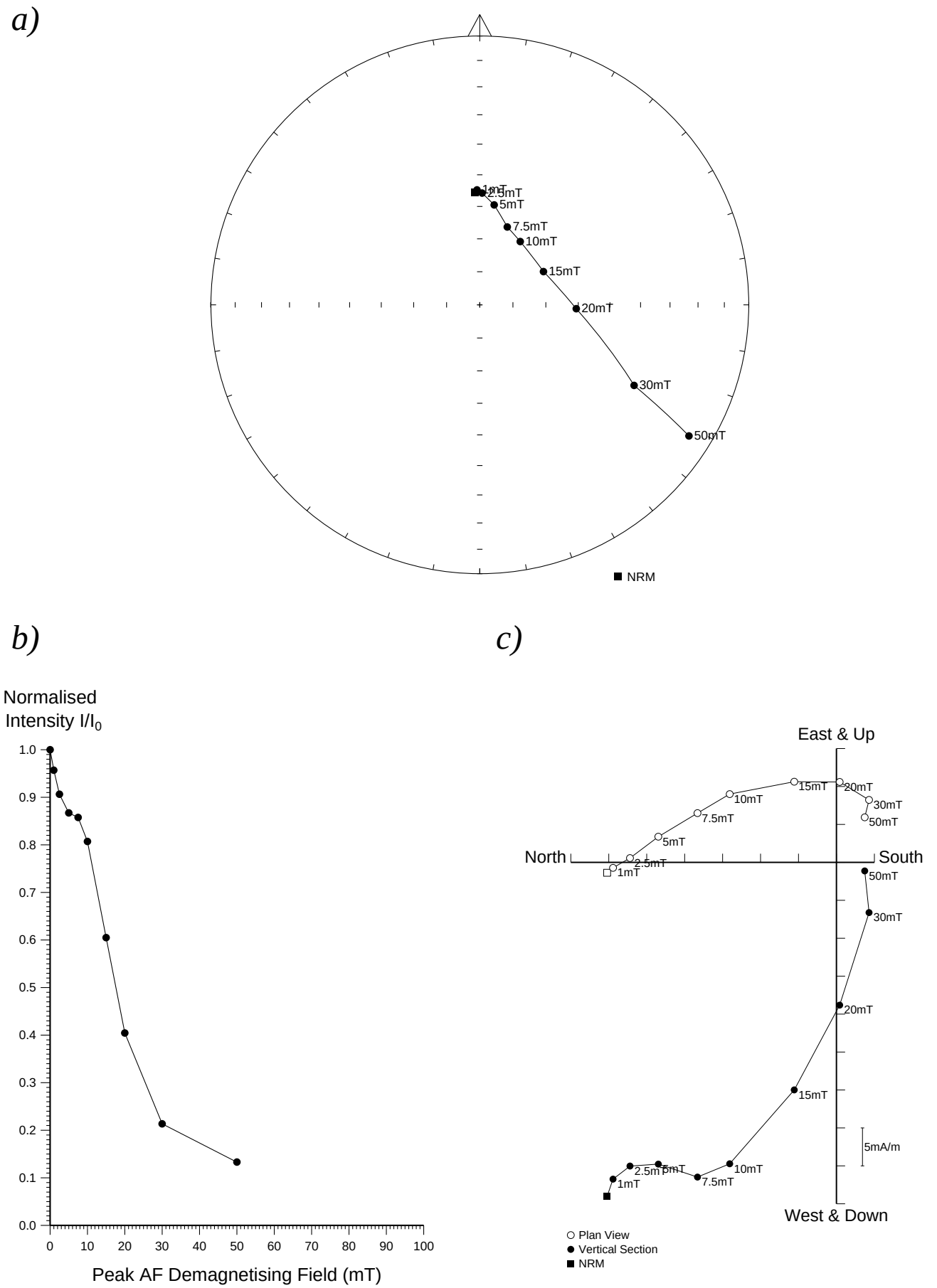

Figure 25: Stepwise AF demagnetisation of sample 18BP13. Diagram a) depicts the variation of the remanent direction as an equal area stereogram (declination increases clockwise, while inclination increases from zero at the equator to 90 degrees at the centre of the projection); b) shows the normalised change in remanence intensity as a function of the demagnetising field; c) shows the changes in both direction and intensity as a vector endpoint projection.

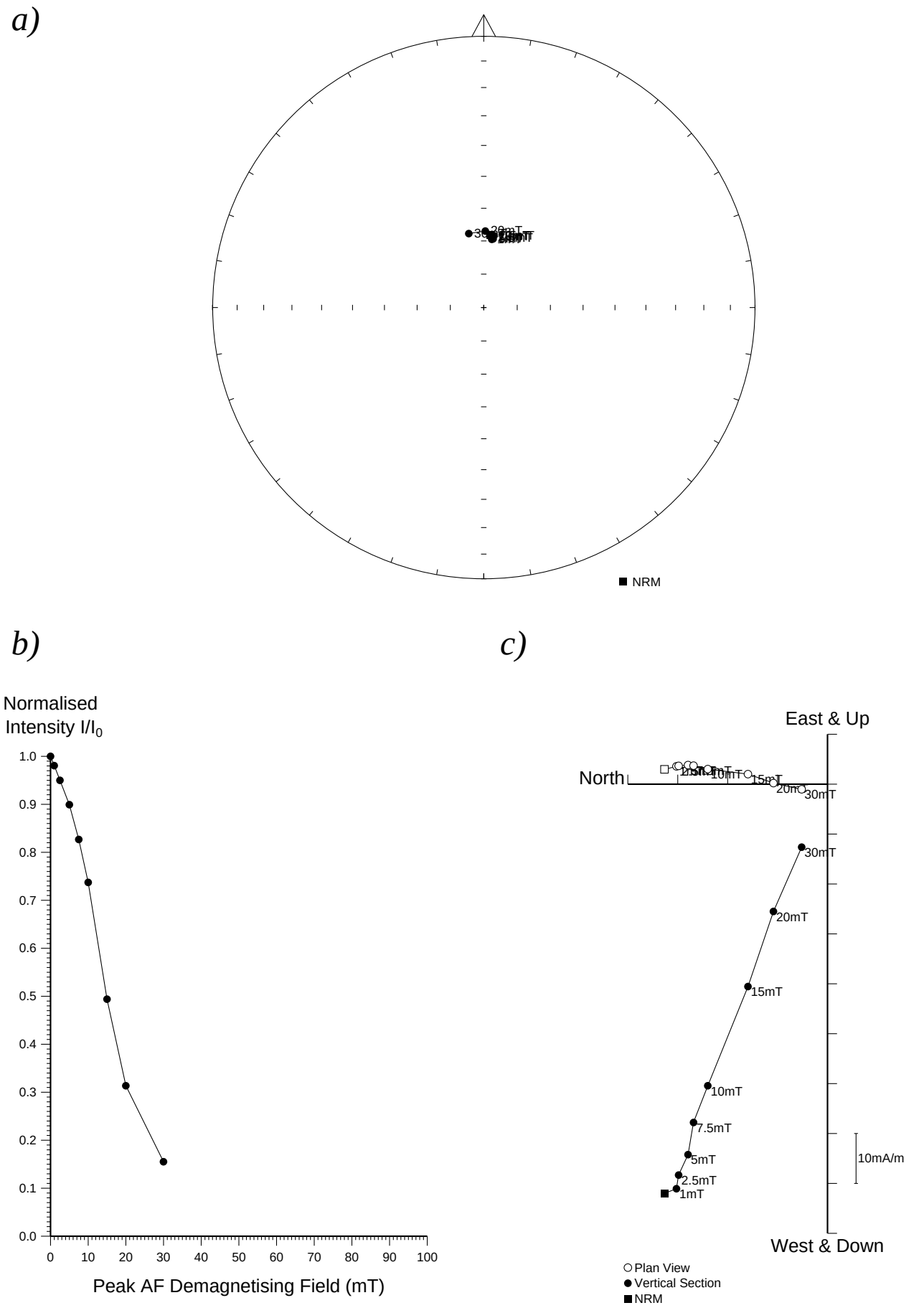

Figure 24: Stepwise AF demagnetisation of sample 18BP08. Diagram a) depicts the variation of the remanent direction as an equal area stereogram (declination increases clockwise, while inclination increases from zero at the equator to 90 degrees at the centre of the projection); b) shows the normalised change in remanence intensity as a function of the demagnetising field; c) shows the changes in both direction and intensity as a vector endpoint projection.

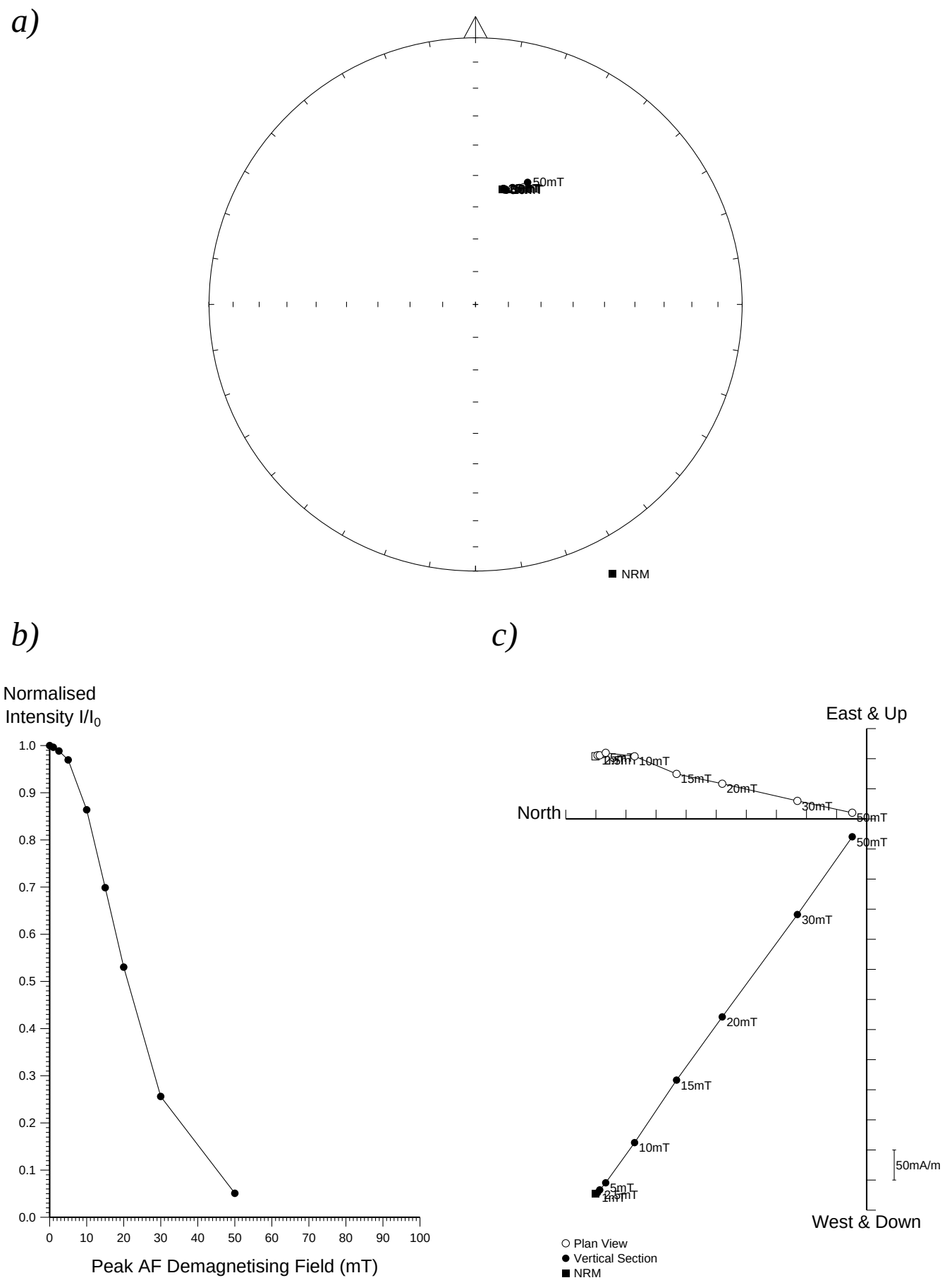

Figure 23: Stepwise AF demagnetisation of sample 18BP06. Diagram a) depicts the variation of the remanent direction as an equal area stereogram (declination increases clockwise, while inclination increases from zero at the equator to 90 degrees at the centre of the projection); b) shows the normalised change in remanence intensity as a function of the demagnetising field; c) shows the changes in both direction and intensity as a vector endpoint projection.

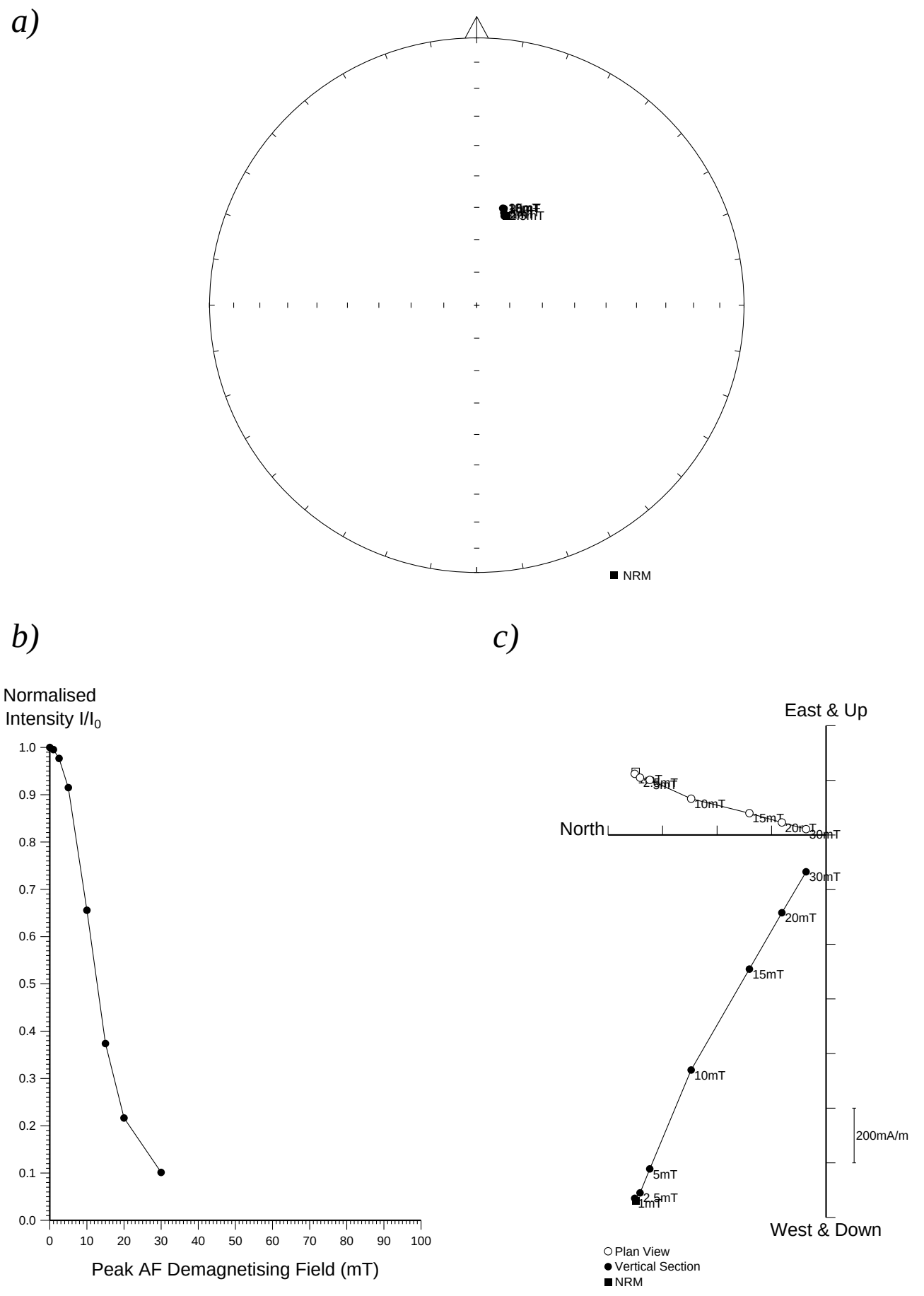

Figure 22: Stepwise AF demagnetisation of sample 18BP03. Diagram a) depicts the variation of the remanent direction as an equal area stereogram (declination increases clockwise, while inclination increases from zero at the equator to 90 degrees at the centre of the projection); b) shows the normalised change in remanence intensity as a function of the demagnetising field; c) shows the changes in both direction and intensity as a vector endpoint projection.

a)

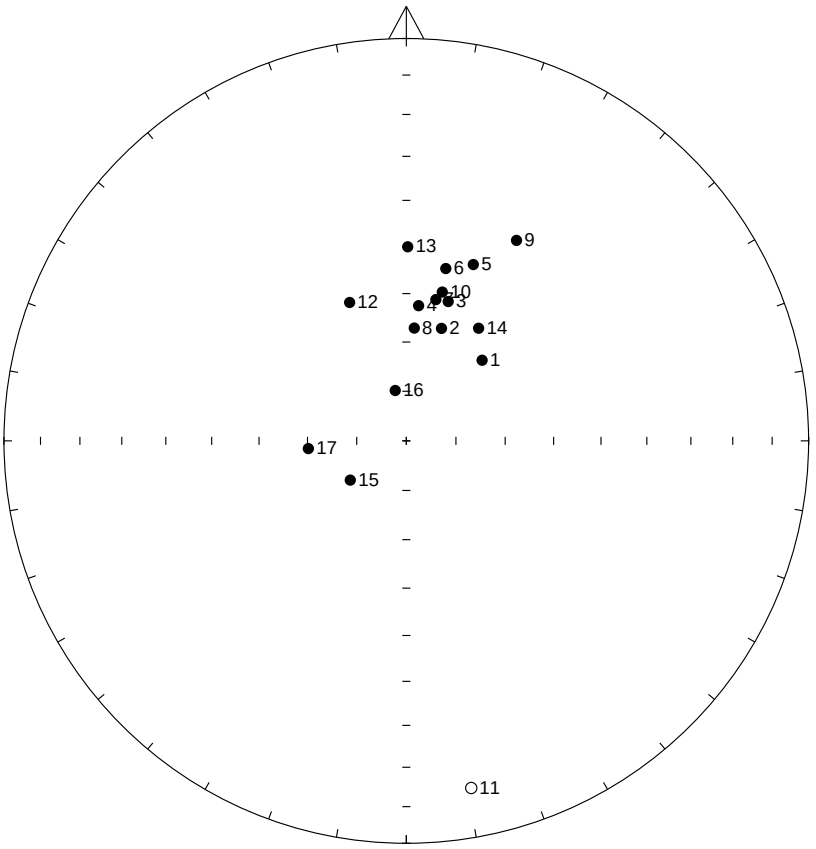

b)

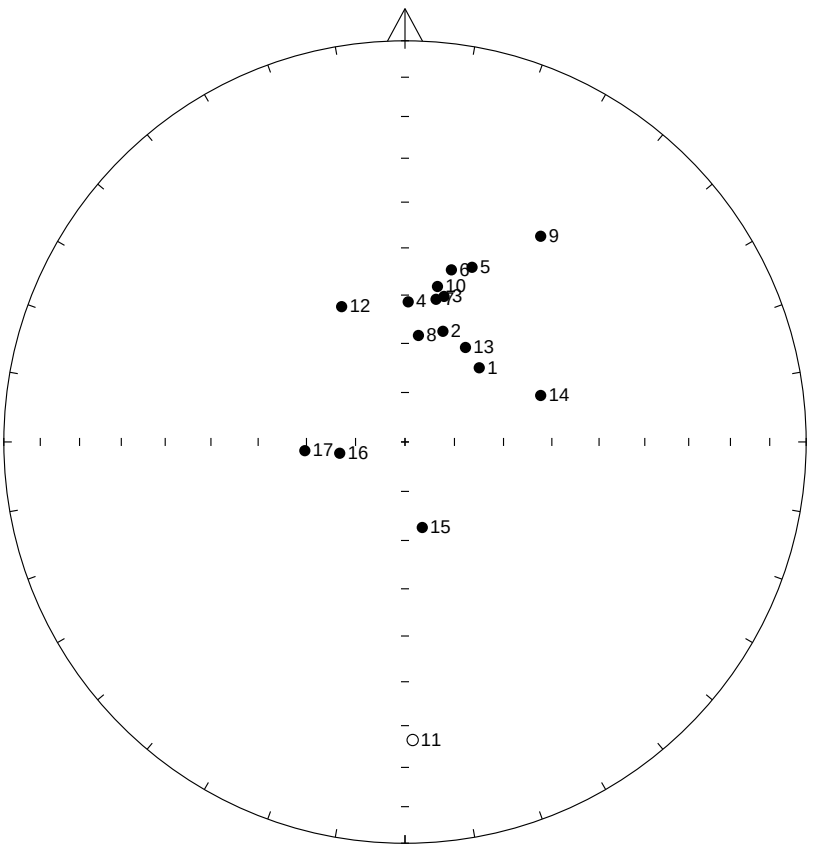

Figure 21: a) Distribution of NRM directions of samples from feature 18BP represented as an equal area stereogram. In this projection declination increases clockwise with zero being at 12 o'clock while inclination increases from zero at the equator to 90 degrees in the centre of the projection. Open circles represent negative inclinations. b) Distribution of thermoremanent directions of magnetisation of the same samples after partial AF demagnetisation to 10mT.

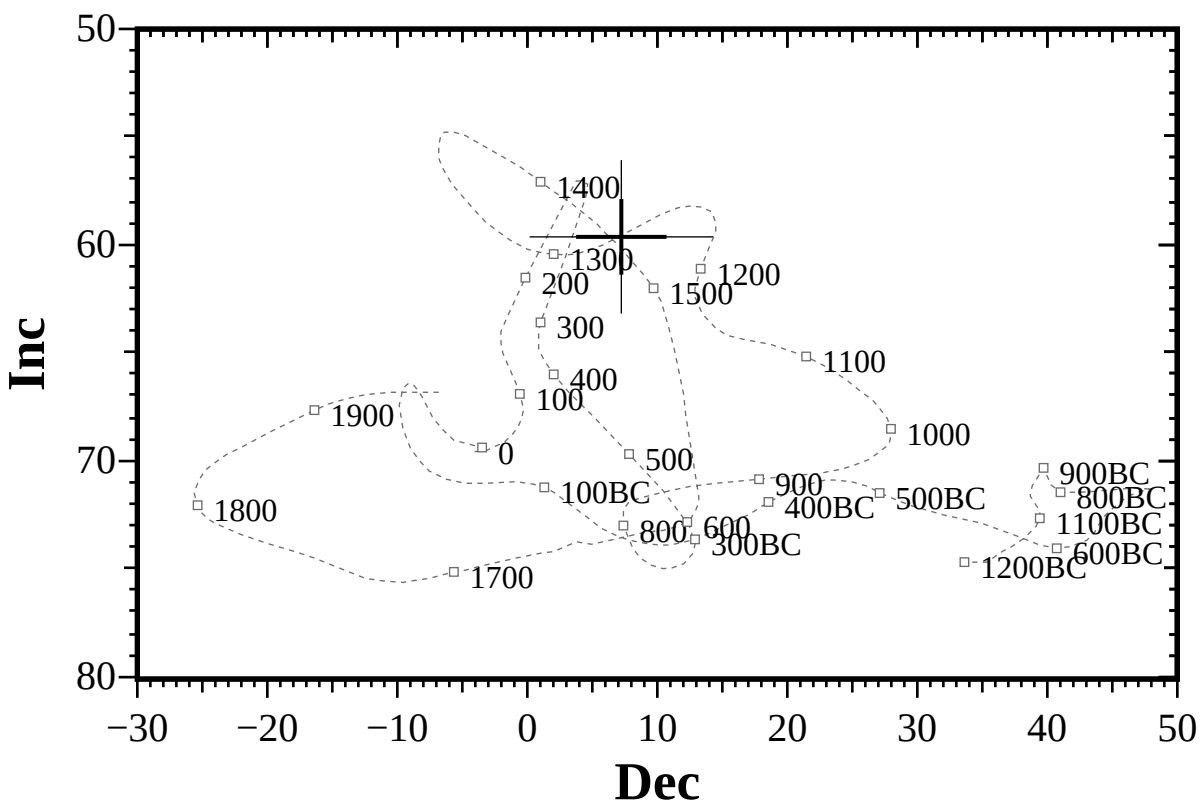

Figure 20: Comparison of the mean thermoremanent vector calculated from samples 04-05, 07, 09, 11 and 14 from feature 17BP after 15mT partial demagnetisation with the UK master calibration curve. Thick error bar lines represent 63% confidence limits and narrow lines 95% confidence limits.

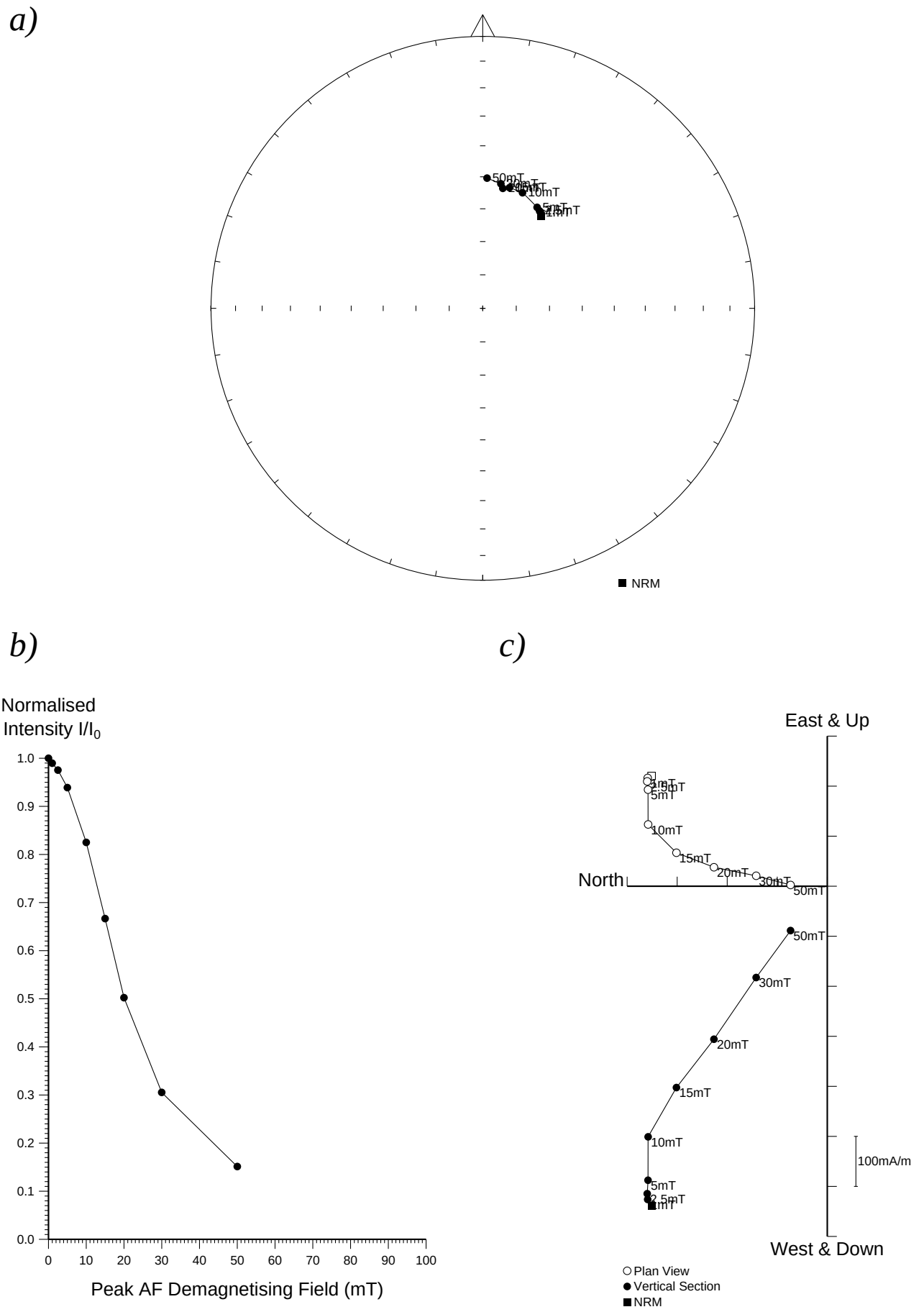

Figure 19: Stepwise AF demagnetisation of sample 17BP14. Diagram a) depicts the variation of the remanent direction as an equal area stereogram (declination increases clockwise, while inclination increases from zero at the equator to 90 degrees at the centre of the projection); b) shows the normalised change in remanence intensity as a function of the demagnetising field; c) shows the changes in both direction and intensity as a vector endpoint projection.

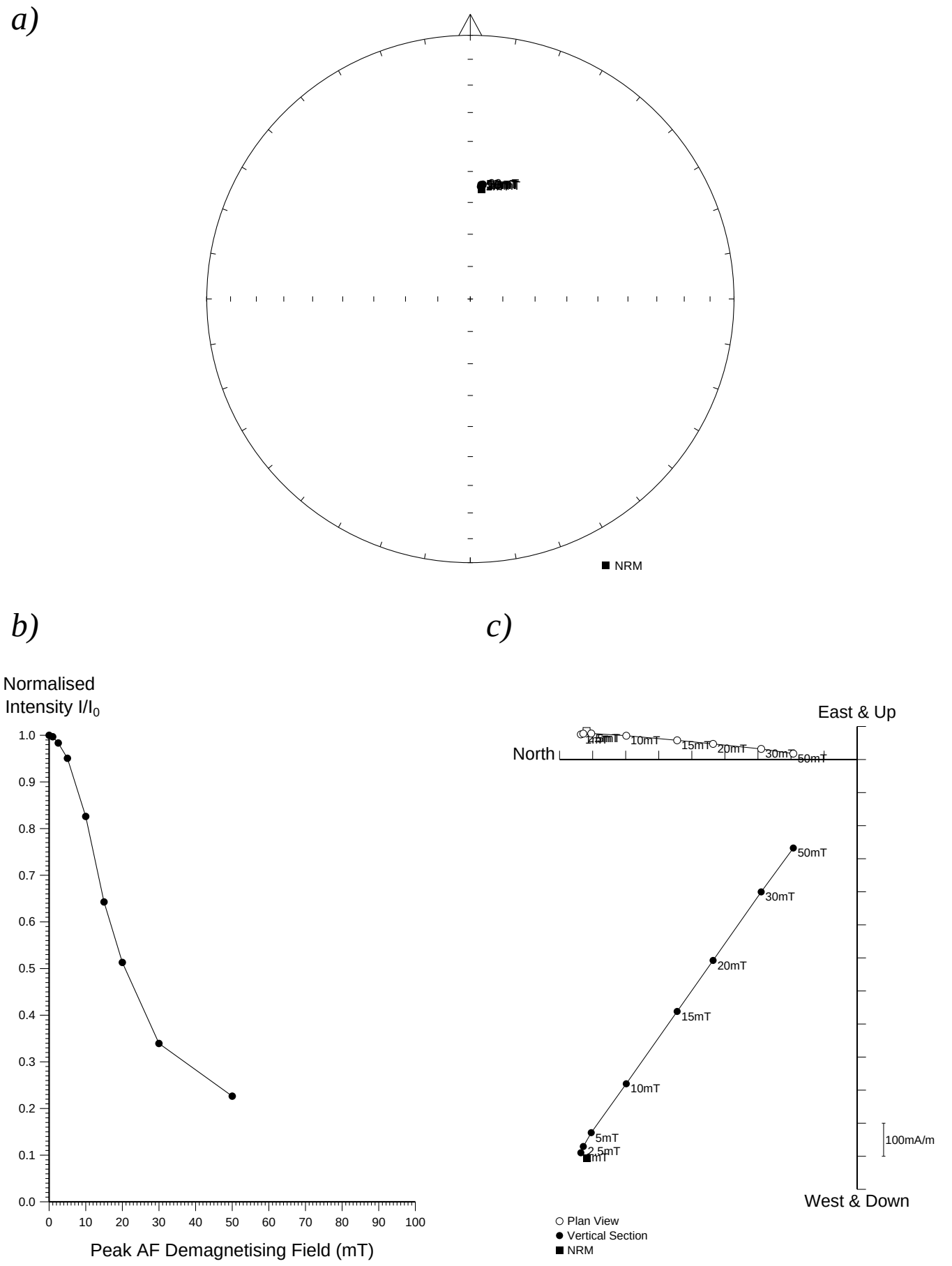

Figure 18: Stepwise AF demagnetisation of sample 17BP11. Diagram a) depicts the variation of the remanent direction as an equal area stereogram (declination increases clockwise, while inclination increases from zero at the equator to 90 degrees at the centre of the projection); b) shows the normalised change in remanence intensity as a function of the demagnetising field; c) shows the changes in both direction and intensity as a vector endpoint projection.

a)

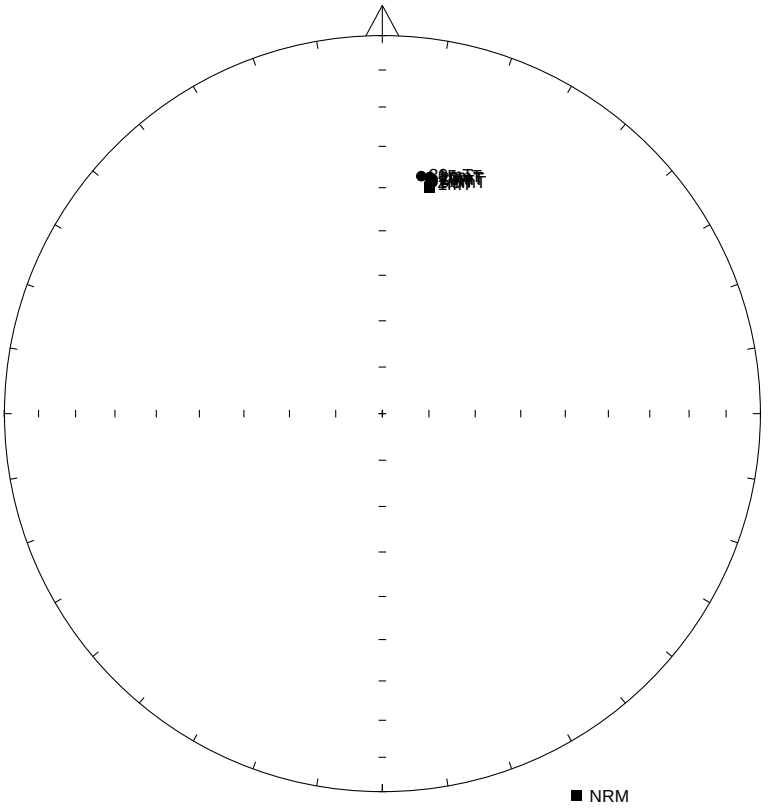

b)

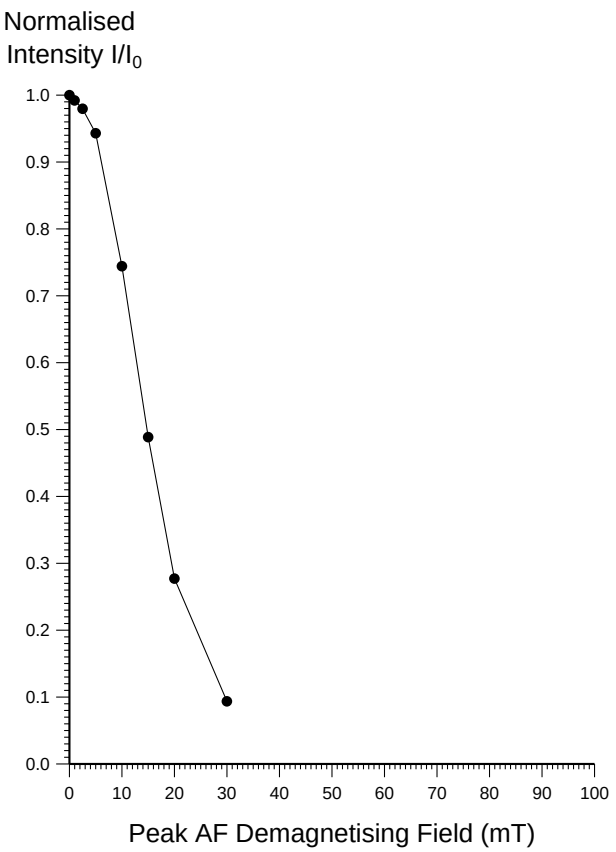

c)

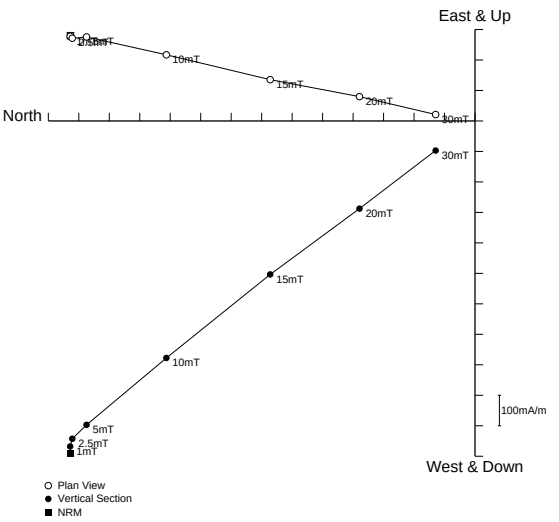

Figure 17: Stepwise AF demagnetisation of sample 17BP06. Diagram a) depicts the variation of the remanent direction as an equal area stereogram (declination increases clockwise, while inclination increases from zero at the equator to 90 degrees at the centre of the projection); b) shows the normalised change in remanence intensity as a function of the demagnetising field; c) shows the changes in both direction and intensity as a vector endpoint projection.

a)

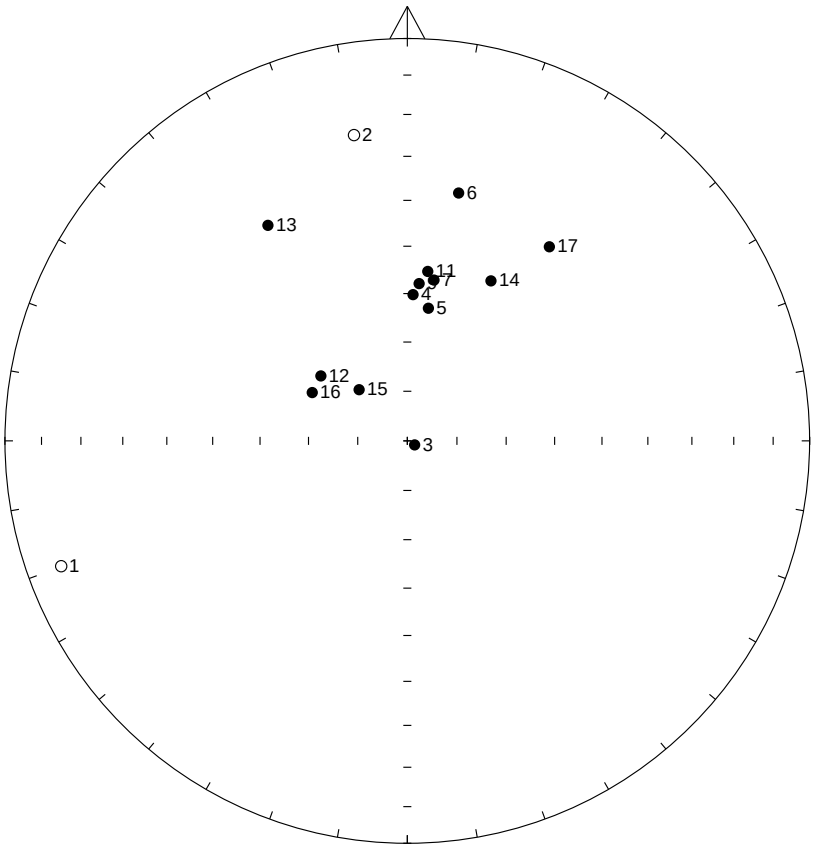

b)

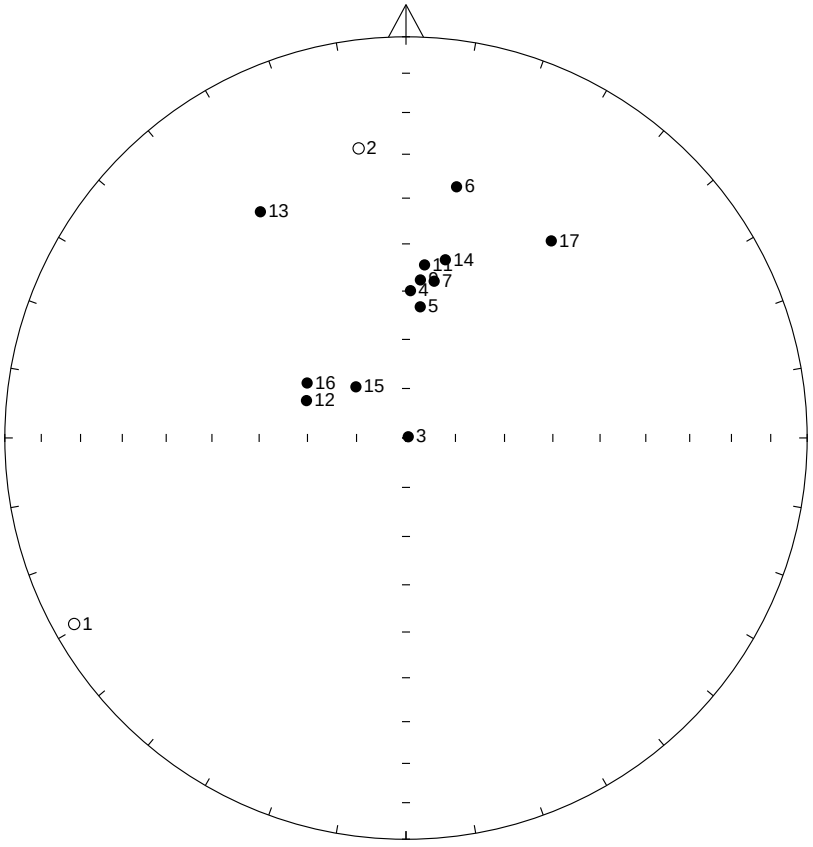

Figure 16: a) Distribution of NRM directions of samples from feature 17BP represented as an equal area stereogram. In this projection declination increases clockwise with zero being at 12 o'clock while inclination increases from zero at the equator to 90 degrees in the centre of the projection. Open circles represent negative inclinations. b) Distribution of thermoremanent directions of magnetisation of the same samples after partial AF demagnetisation to 15mT.

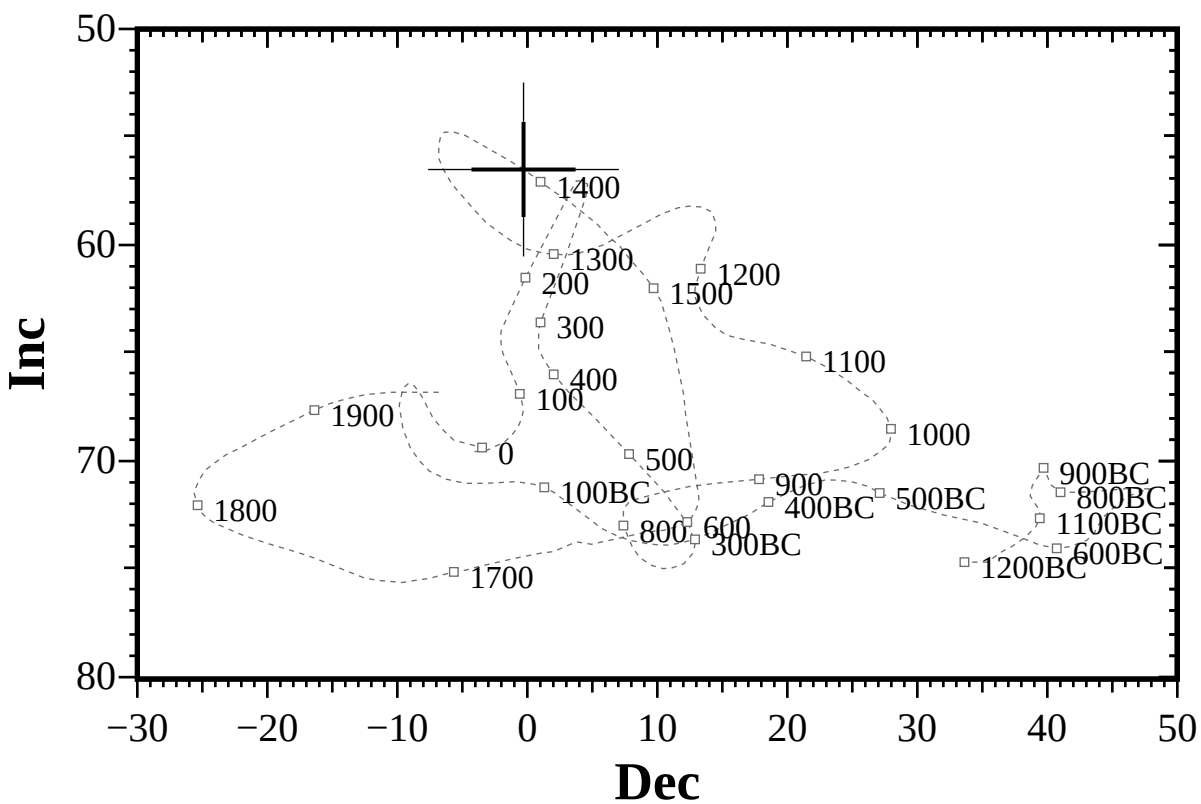

Figure 15: Comparison of the mean thermoremanent vector calculated from samples 01-03, 06-10 and 12-19 from feature 15BBP after 5mT partial demagnetisation with the UK master calibration curve. Thick error bar lines represent 63% confidence limits and narrow lines 95% confidence limits.

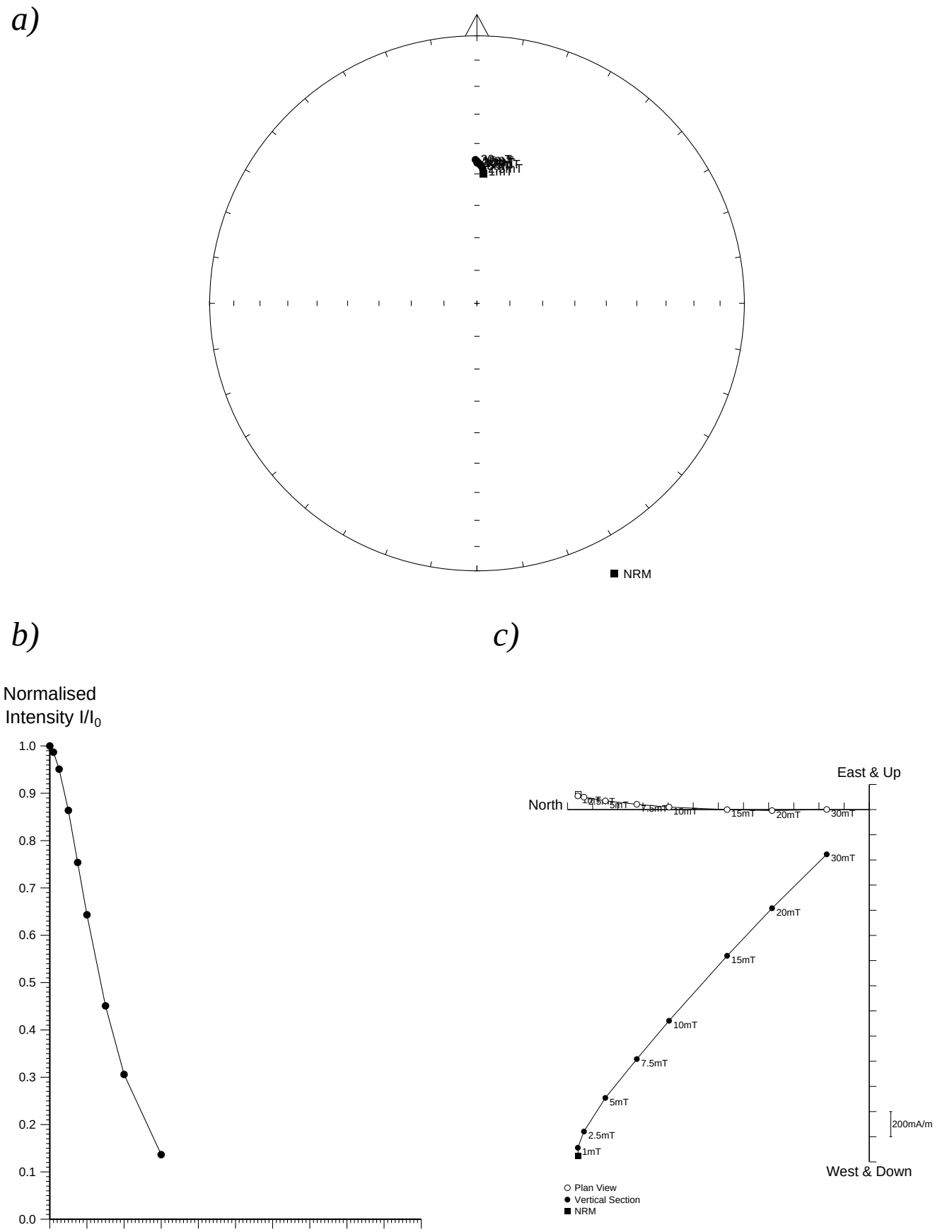

Figure 14: Stepwise AF demagnetisation of sample 15BBP16. Diagram a) depicts the variation of the remanent direction as an equal area stereogram (declination increases clockwise, while inclination increases from zero at the equator to 90 degrees at the centre of the projection); b) shows the normalised change in remanence intensity as a function of the demagnetising field; c) shows the changes in both direction and intensity as a vector endpoint projection.

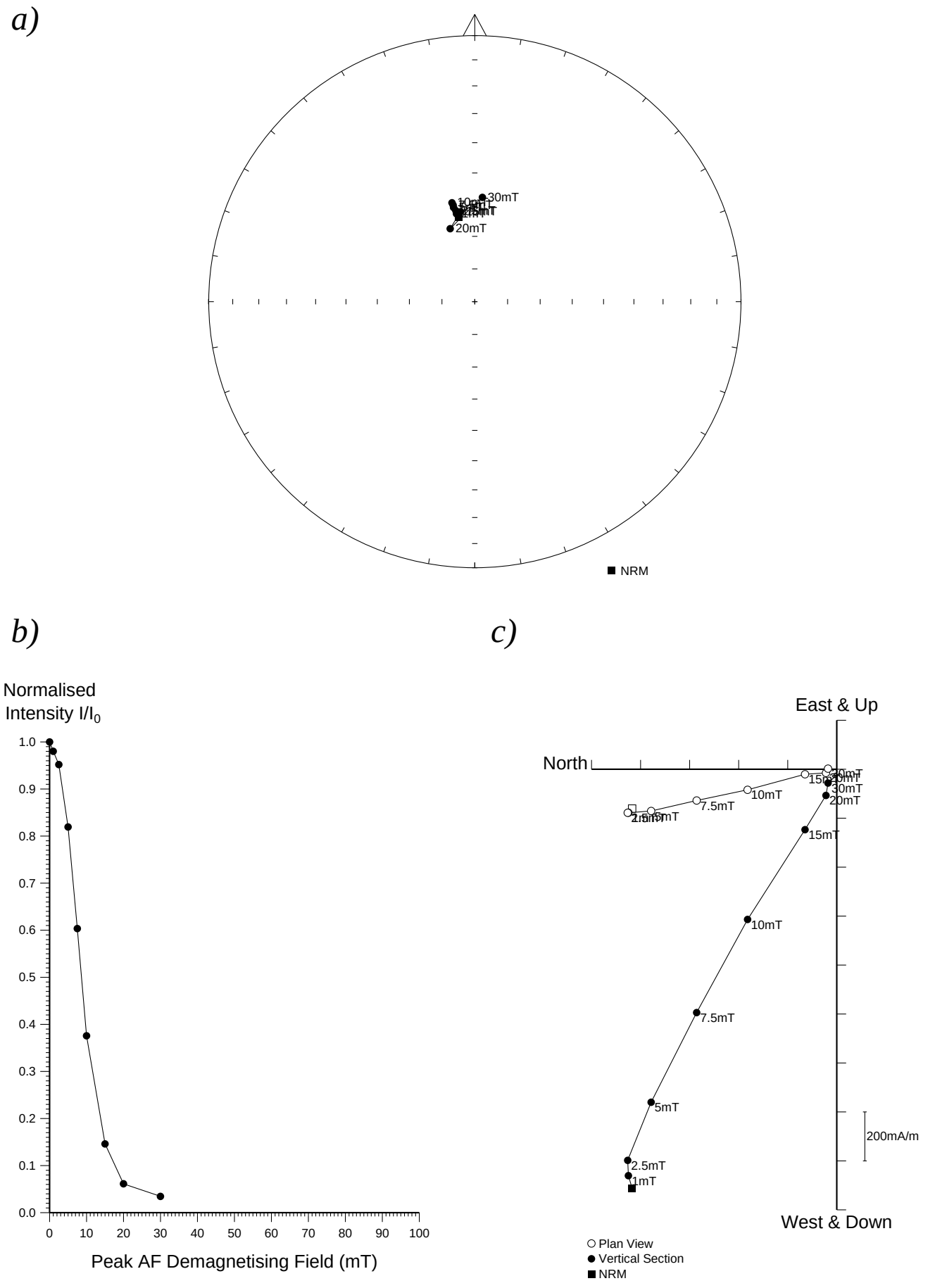

Figure 13: Stepwise AF demagnetisation of sample 15BBP09. Diagram a) depicts the variation of the remanent direction as an equal area stereogram (declination increases clockwise, while inclination increases from zero at the equator to 90 degrees at the centre of the projection); b) shows the normalised change in remanence intensity as a function of the demagnetising field; c) shows the changes in both direction and intensity as a vector endpoint projection.

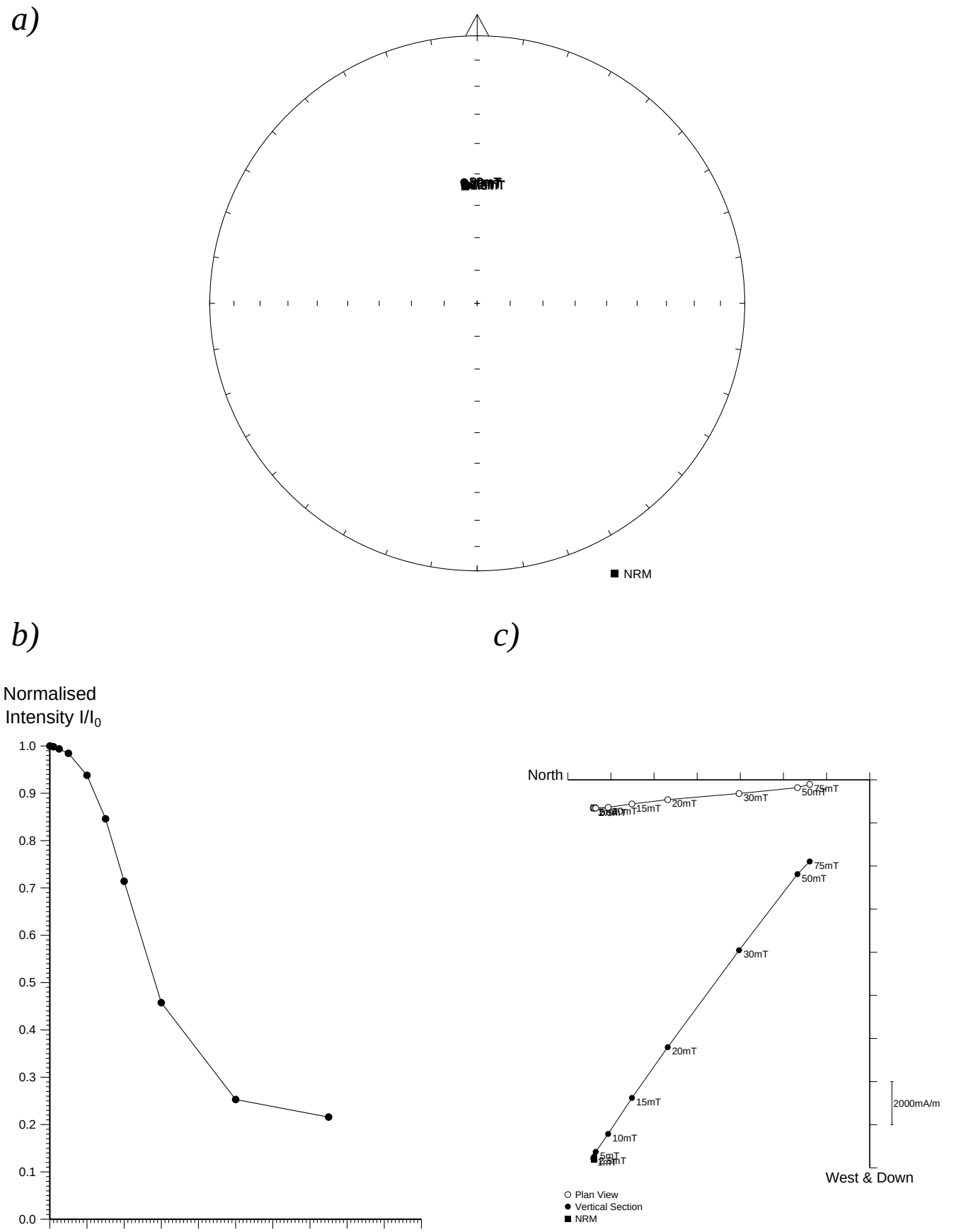

Figure 12: Stepwise AF demagnetisation of sample 15BBP01. Diagram a) depicts the variation of the remanent direction as an equal area stereogram (declination increases clockwise, while inclination increases from zero at the equator to 90 degrees at the centre of the projection); b) shows the normalised change in remanence intensity as a function of the demagnetising field; c) shows the changes in both direction and intensity as a vector endpoint projection.

a)

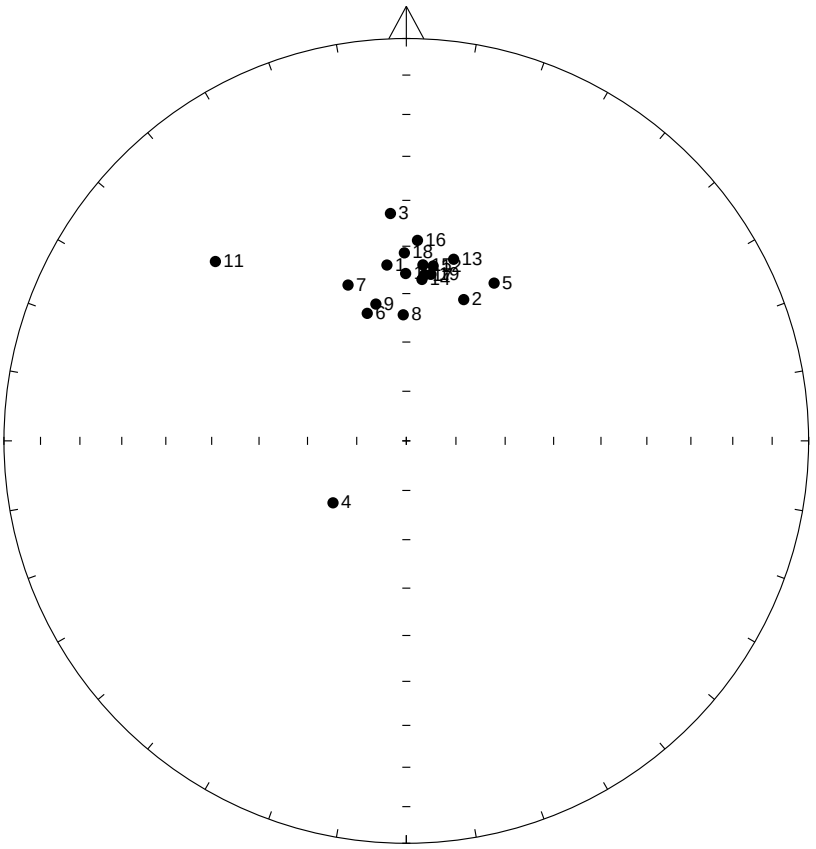

b)

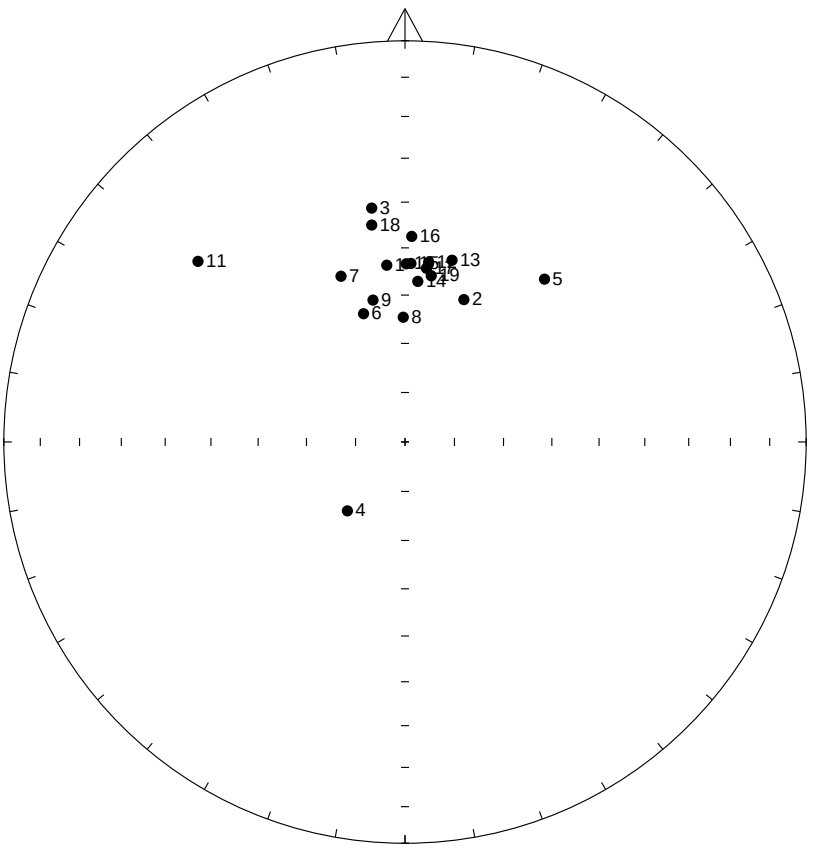

Figure 11: a) Distribution of NRM directions of samples from feature 15BBP represented as an equal area stereogram. In this projection declination increases clockwise with zero being at 12 o'clock while inclination increases from zero at the equator to 90 degrees in the centre of the projection. Open circles represent negative inclinations. b) Distribution of thermoremanent directions of magnetisation of the same samples after partial AF demagnetisation to 5mT.

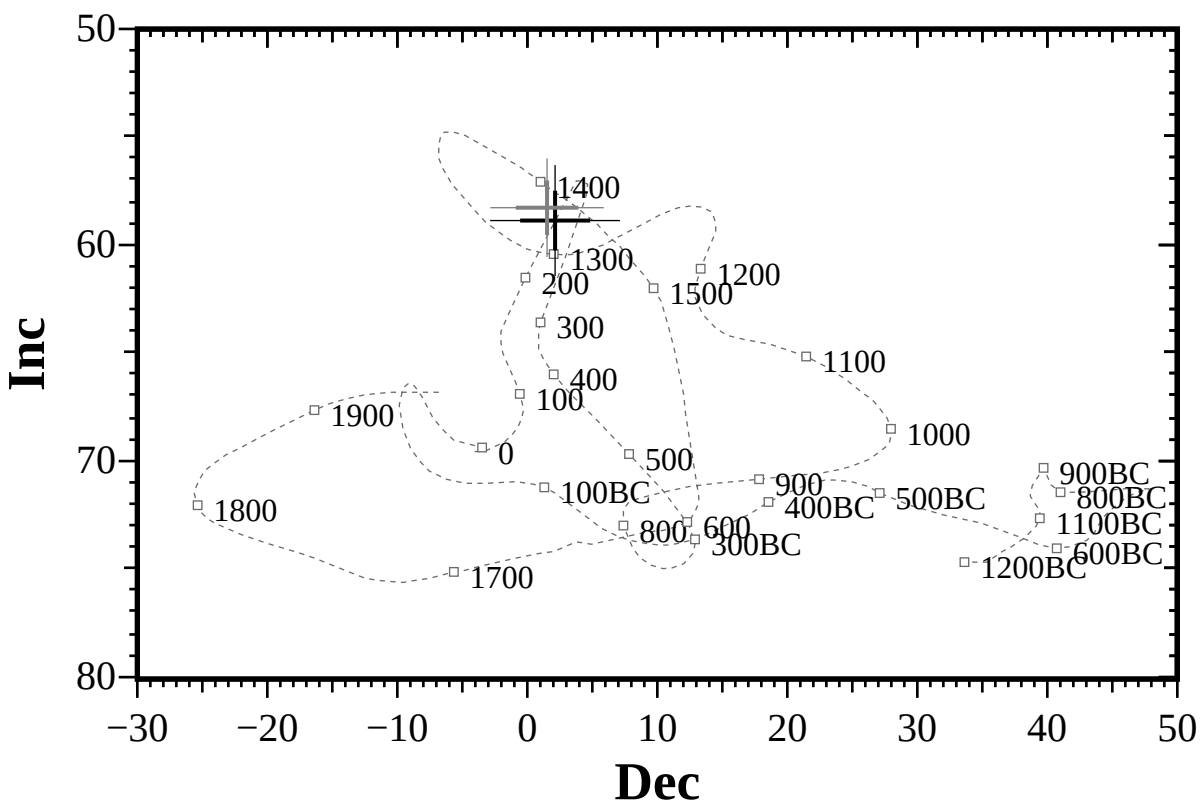

Figure 10: Comparison of the mean thermoremanent vector calculated from samples 01, 03-06, 08-09, 11, 13-15 and 18 from feature 6ABP after 15mT partial demagnetisation with the UK master calibration curve (black cross). The grey cross represents the mean TRM calculated by combining these samples with those taken in 2000. Thick error bar lines represent 63% confidence limits and narrow lines 95% confidence limits.

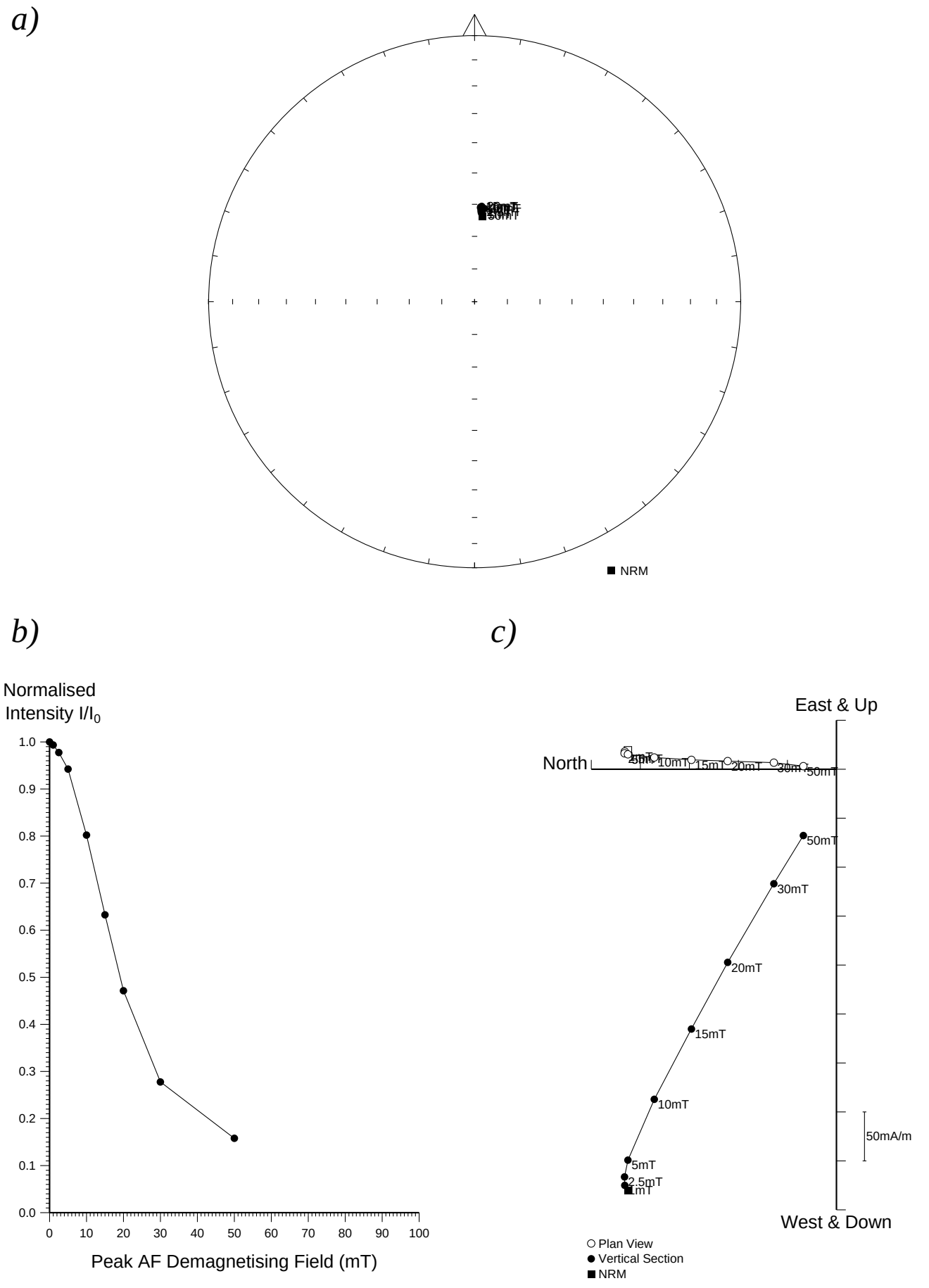

Figure 9: Stepwise AF demagnetisation of sample 6ABP14. Diagram a) depicts the variation of the remanent direction as an equal area stereogram (declination increases clockwise, while inclination increases from zero at the equator to 90 degrees at the centre of the projection); b) shows the normalised change in remanence intensity as a function of the demagnetising field; c) shows the changes in both direction and intensity as a vector endpoint projection.

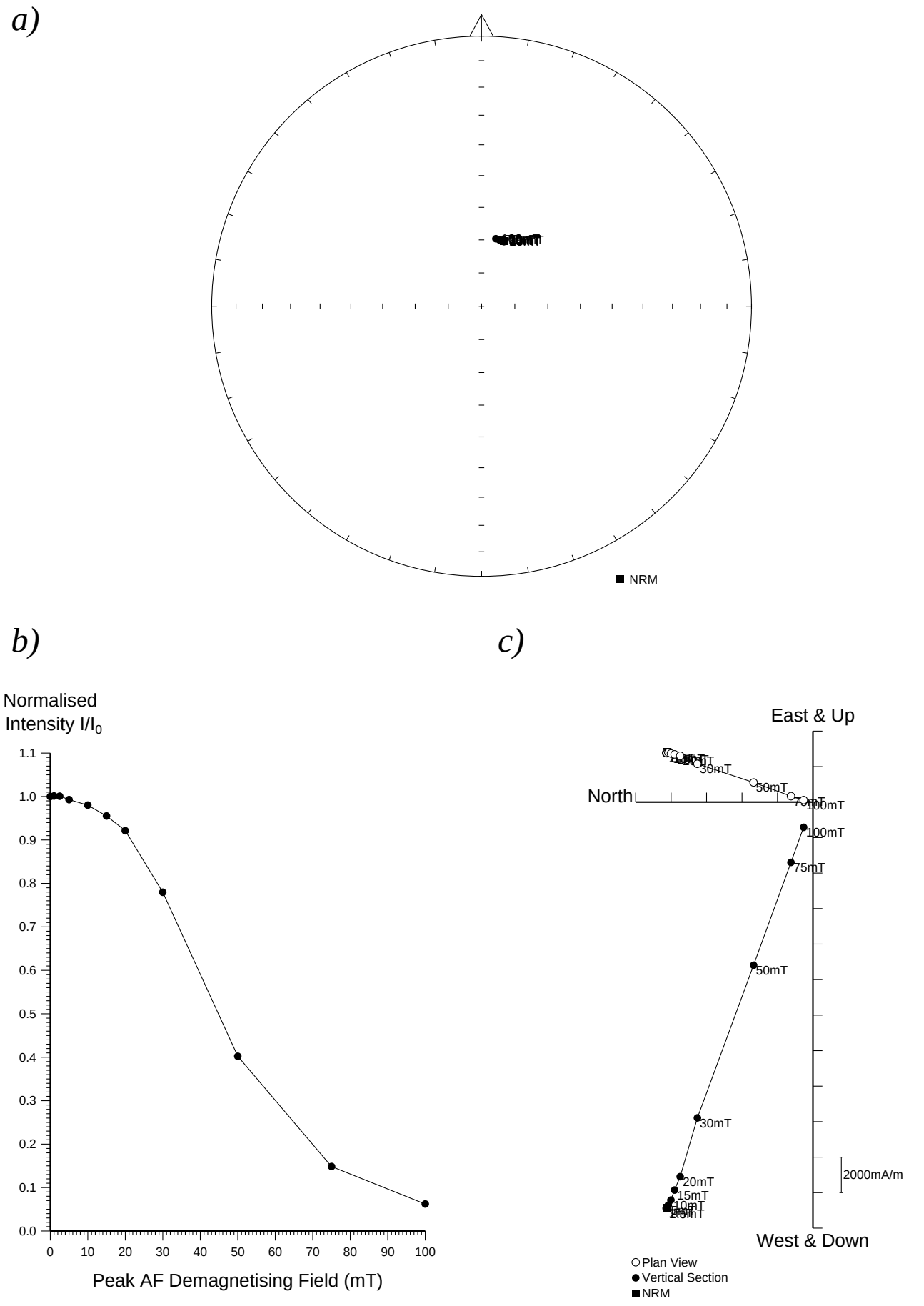

Figure 8: Stepwise AF demagnetisation of sample 6ABP12. Diagram a) depicts the variation of the remanent direction as an equal area stereogram (declination increases clockwise, while inclination increases from zero at the equator to 90 degrees at the centre of the projection); b) shows the normalised change in remanence intensity as a function of the demagnetising field; c) shows the changes in both direction and intensity as a vector endpoint projection.

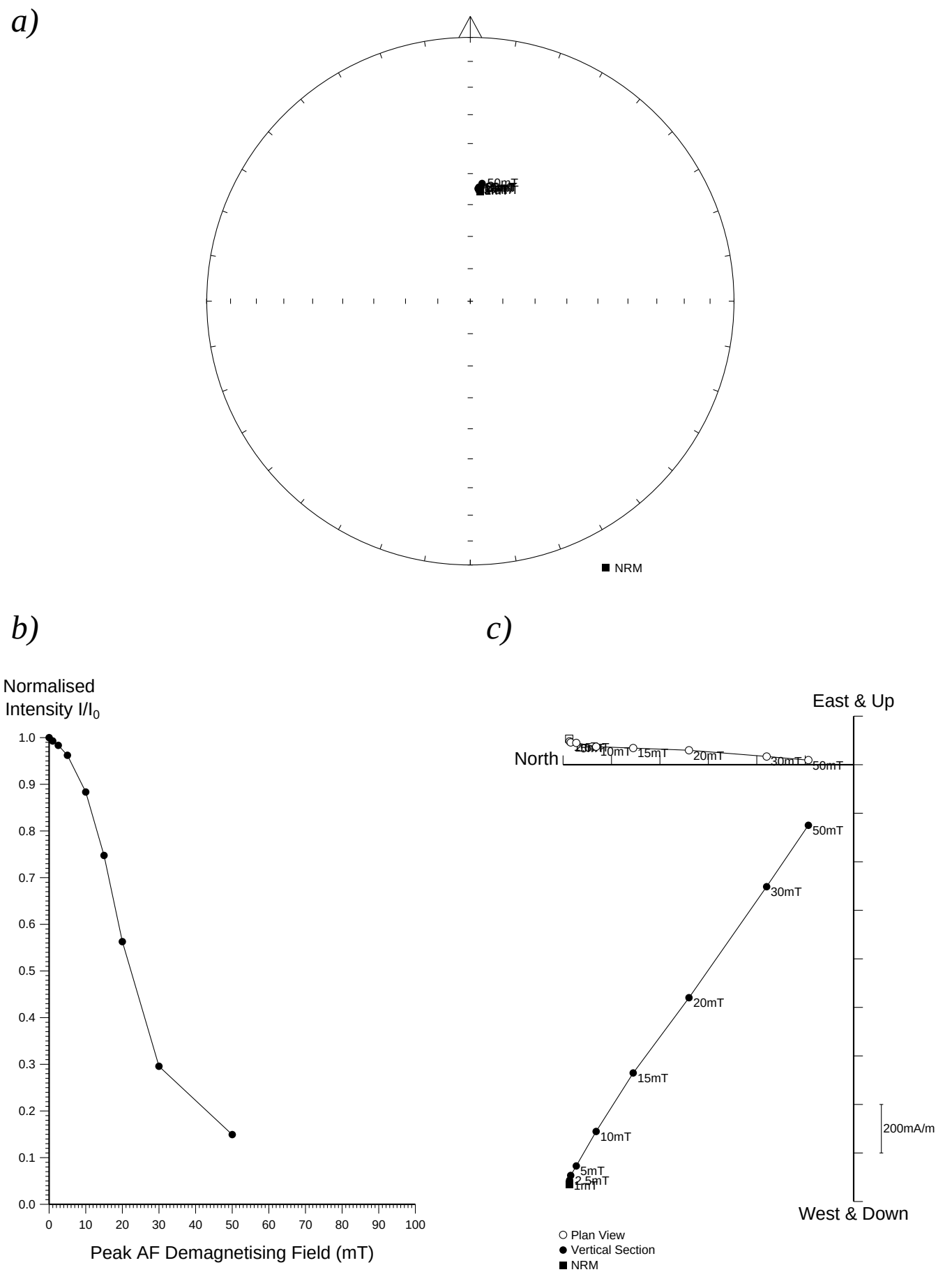

Figure 7: Stepwise AF demagnetisation of sample 6ABP03. Diagram a) depicts the variation of the remanent direction as an equal area stereogram (declination increases clockwise, while inclination increases from zero at the equator to 90 degrees at the centre of the projection); b) shows the normalised change in remanence intensity as a function of the demagnetising field; c) shows the changes in both direction and intensity as a vector endpoint projection.

a)

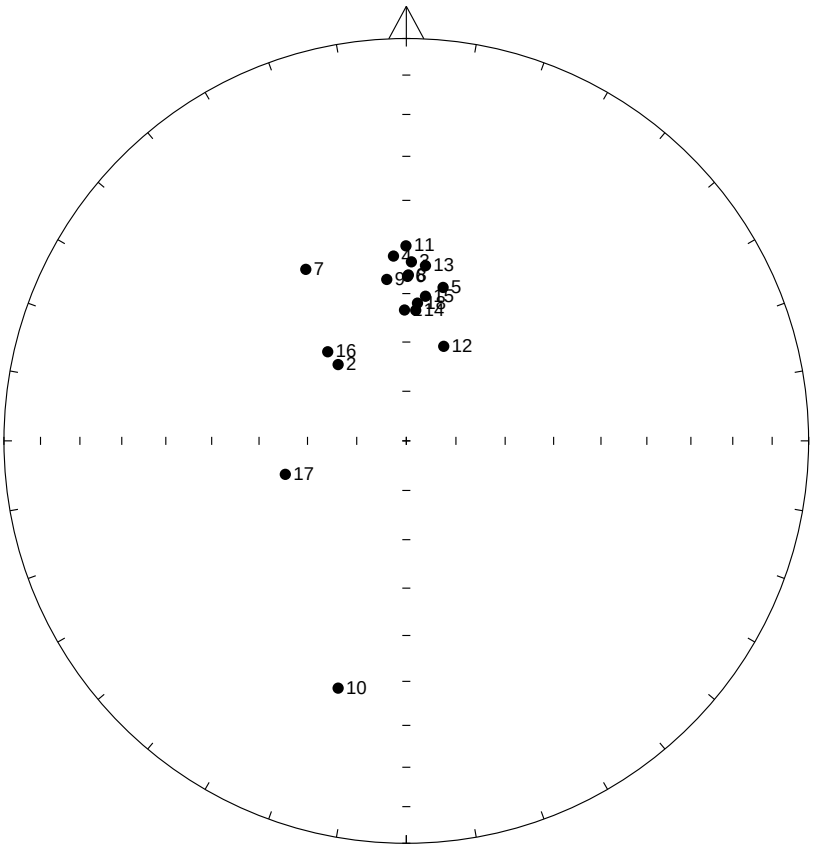

b)

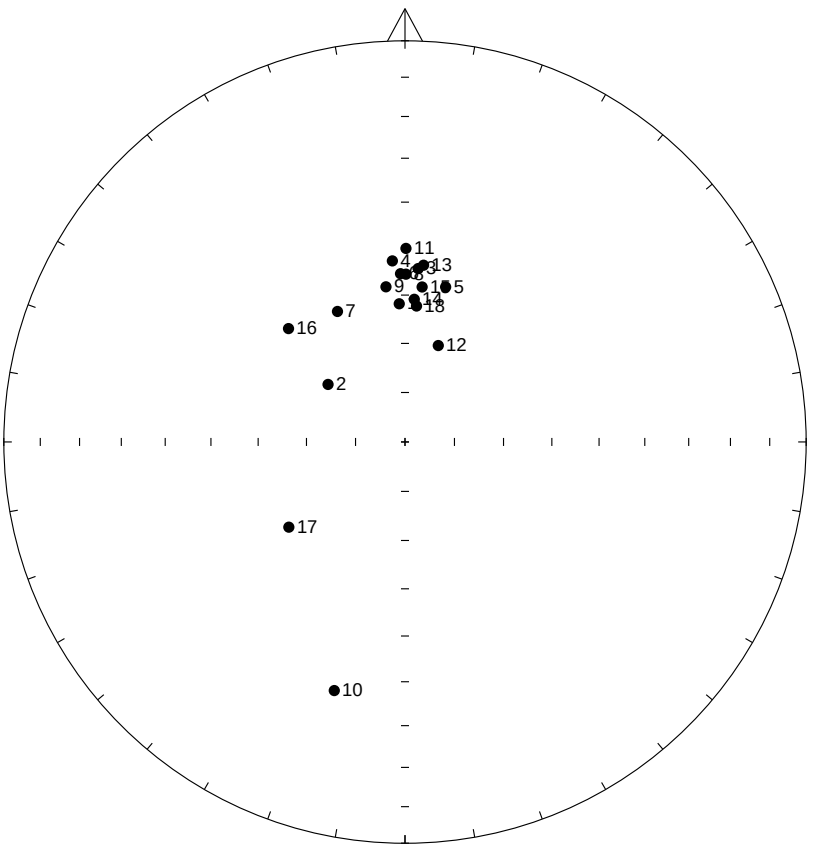

Figure 6: a) Distribution of NRM directions of samples from feature 6ABP represented as an equal area stereogram. In this projection declination increases clockwise with zero being at 12 o'clock while inclination increases from zero at the equator to 90 degrees in the centre of the projection. Open circles represent negative inclinations. b) Distribution of thermoremanent directions of magnetisation of the same samples after partial AF demagnetisation to 15mT.

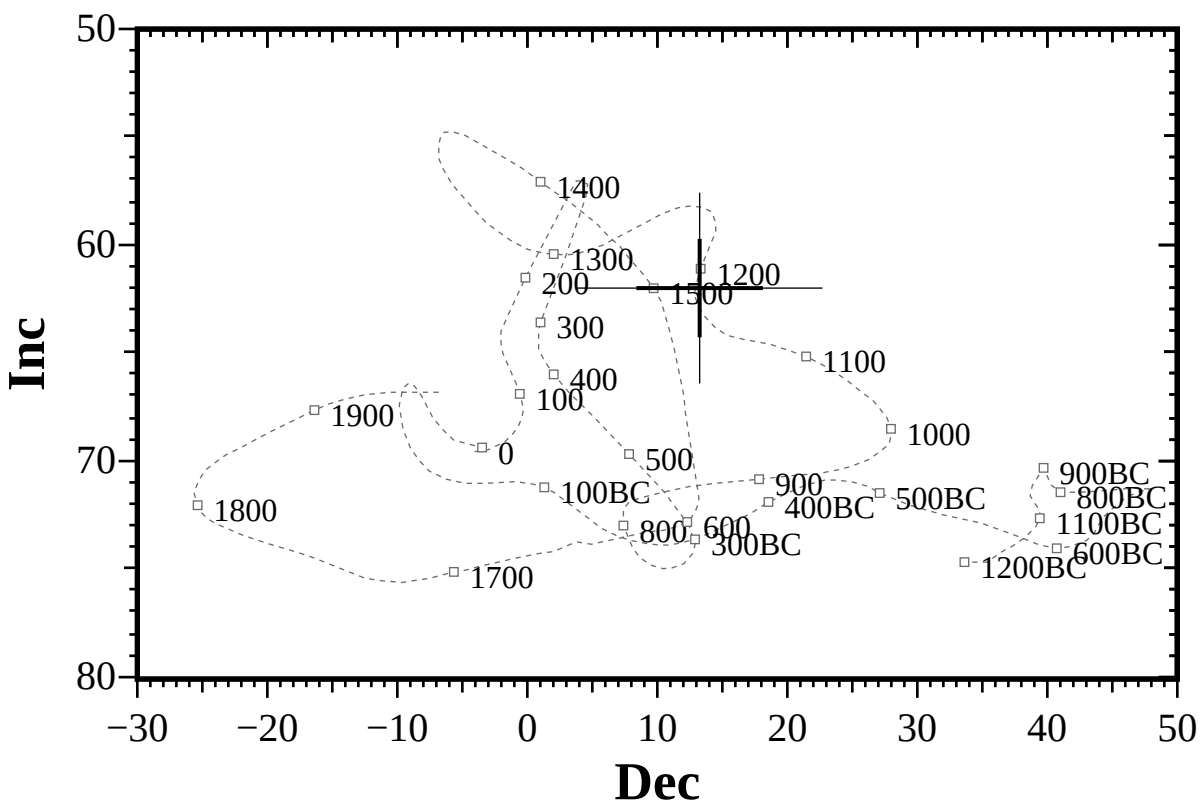

Figure 27: Comparison of the mean thermoremanent vector calculated from samples 02-08 and 10 from feature 18BP after 10mT partial demagnetisation with the UK master calibration curve. Thick error bar lines represent 63% confidence limits and narrow lines 95% confidence limits.